Master's thesis

NTNU
Norwegian University of Science and Technology
Faculty of Natural Sciences
Department of Biotechnology and Food Science

Marita Gresseth

Investigating fluorescence in transformants expressing a silicanin-mNeonGreen fusion protein, and the effect of cytoskeleton inhibitors on frustule biosynthesis in the diatom *Thalassiosira pseudonana*

Master's thesis in Industrial Chemistry and Biotechnology
Supervisor: Olav Vadstein, Tore Brembu
July 2020

NTNU
Norwegian University of
Science and Technology

Marita Gresseth

Investigating fluorescence in transformants expressing a silicanin-mNeonGreen fusion protein, and the effect of cytoskeleton inhibitors on frustule biosynthesis in the diatom *Thalassiosira pseudonana*

Master's thesis in Industrial Chemistry and Biotechnology
Supervisor: Olav Vadstein, Tore Brembu
July 2020

Norwegian University of Science and Technology
Faculty of Natural Sciences
Department of Biotechnology and Food Science

NTNU
Norwegian University of
Science and Technology

Acknowledgements

This master's thesis was carried out at the Department of Biotechnology and Food Science at the Norwegian University of Science and Technology in the period from January to July of 2020.

I would like to thank my supervisors Olav Vadstein and Tore Brembu for all their help and support during this last year. Also, thanks to Marthe Hafskjold and Annika Messemer for all your assistance in the lab, and for taking care of my algae when I was unable to be there. Thank you to Thi My Linh Hoang for your help imaging in SEM.

Thanks to Randi Sund and Hanne Dalsvåg who have helped me through the past 5 years with your love, support and comic relief. I would also like to thank Vilde Årdal, who has been standing beside me through all the joys and hardships of this thesis and who I could always count on to join me for coffee and a good talk. Lastly, I would like to thank all my other friends and family for your encouragement and loving words.

Abstract

Diatoms are ubiquitous microorganisms that have unique cell walls made from silica called frustules. These frustules have intricate species-specific patterns, and are known for their high specific strength. By understanding the formation of the frustule, it is believed that one can gain precious information about how to make materials with the same qualities, which can be utilised in nanotechnological applications. A previous thesis made fluorescent mNeonGreen-Tp24711 fusion gene transformants of *Thalassiosira pseudonana* in order to study the location and expression of the silicanin Tp24711, however, the cells stopped expressing the gene afterwards. This study aims to understand what happened to the transformants, in addition to investigating how cytoskeleton inhibitors affect valve morphology in *T. pseudonana*. Furthermore, the thesis takes a comprehensive look on existing research on proteins and organic molecules that are involved in frustule synthesis in diatoms, through a literature study. The transformants that stopped expressing fluorescence were studied through microscopy, flow cytometry and western blotting, all of which indicated no expression of mNeonGreen. A PCR was run in order to see if something had happened to the sequence on the plasmid, but the results were inconclusive. At the end of the thesis the transformants were reobserved using fluorescence and confocal microscopy, which showed that they had regained their mNeonGreen fluorescence. After addition of cytoskeleton inhibitors to cultures of *T. pseudonana* the frustules were observed using Scanning Electron Microscopy. Several of the frustules treated with microtubule inhibitors (colchicine and oryzalin) showed a disordered growth of ribs and cross-links, while several others had almost no growth of ribs and cross-links. The frustules also had irregular numbers of fultoportulae. The frustules that were grown with addition of a microfilament inhibitor (cytochalasin D) lacked protruding ribs and cross-links, and they were missing a fultoportula.

Sammendrag

Kiselalger er utbredte mikroorganismer som har unike cellevegger laget av silika kalt frustuler. Disse frustulene har intrikate, artsspesifikke mønstre, og er spesielt kjente for at de har en høy spesifikk styrke. Ved å forstå frustuleformasjonen i kiselalger er det antatt at man skal kunne få viktig informasjon om hvordan materialer med de samme kvalitetene kan syntetiseres, som videre kan brukes i nanoteknologiske applikasjoner. En tidligere avhandling produserte transformanter av fusjonsgenet mNeonGreen-Tp24711 i *Thalassiosira pseudonana* for å studere lokasjon og ekspresjon av silikaninet Tp24711, men etter avhandlingen sluttet cellene å uttrykke genet. Denne studien har som mål å finne ut hva som skjedde med transformantene, i tillegg til å undersøke hvilken effekt cytoskjelettinhibitorer har på frustulens morfologi i *T. pseudonana*. Videre tar avhandlingen et helhetlig blikk på proteiner og organiske molekyler som er involvert i frustulesyntesen i kiselalger i form av et litteraturstudie. Cellene som sluttet å uttrykke fluorescens ble studert gjennom mikroskopi, flowcytometri og western blotting, der alle metodene indikerte at cellene ikke uttrykte mNeonGreen. En PCR-reaksjon ble kjørt for å undersøke om noe hadde skjedd med det transformerte plasmidet, men det var ikke mulig å trekke slutninger rundt resultatet. Ved enden av studien ble algene studert på nytt i fluorescens- og konfokalmikroskop, og da uttrykte de mNeonGreen-fluorescens igjen. Etter tilsats av cytoskjelettinhibitorer til kiselalgekulturer ble frustulene observert i et skanningelektronmikroskop. Frustulene som var behandlet med microtubulus-inhibitorer (colchicine og oryzalin) hadde uorganisert vekst av ribber og krysslinker, samtidig som noen nesten ikke hadde vekst av ribber og krysslinker. Flere av frustulene hadde et uregelmessig antall fultoportulae. Frustulene som var påvirket av en mikrofilament-inhibitor (cytochalasin D) hadde ikke ribber og krysslinker som vokste ut fra valven, og de manglet en fultoportula.

Abbreviations

AFIM	Ammonium Fluoride Insoluble Material
Cin	Cingulin
DMSO	Dimethyl sulfoxide
EDTA	Ethylenediaminetetraacetic acid
ER	Endoplasmic reticulum
fu	Fluorescene units
Fsc	Forward scatter
Gent	Gentamycin
HPLC	High-performance liquid chromatography
Kan	Kanamycin
LCPA	Long Chain Polyamines
MQ	Water purified using the Milli-Q® Reference Water Purification System
NMR	Nuclear magnetic resonance
Nou	Nourseothricin
OD	Optical density
PAGE	Polyacrylamide Gel Electrophoresis
SAP	Silicalemma-associated protein
PCR	Polymerase chain reaction
PTM	Post-translational modification
RXL	Protease cleavage site
SDS	Sodium dodecyl sulfate
SDV	Silica Deposition Vesicle
SEM	Scanning electron microscopy
Sin	Silicanin
Sil	Silaffin
Tris	Trisaminomethane
W	Tryptophane
Y	Tyrosine

Contents

1 Introduction

1.1 Diatoms

Diatoms are a major group of photosynthetic eukaryotes that are spread across the world's oceans. Their contribution to the world's primary production is estimated to be 20 %, which is the equivalent of all of the planets rain forests combined (Ambrust, 2009). They are also food for other water-living species, being at the base of the marine food chain (Bowler et al., 2010). In addition to being a key component of the marine ecosystem, humans have found ways to utilise the diatoms. A large part of the petroleum reserves on the ocean floor are made from diatoms, and the remains of their cell walls can be used for purposes such as filters and pesticides (Yang et al., 2011; Shah and Khan, 2014). This is due to their cell wall, or frustule, which is composed of silica (SiO_2). The frustule has a high specific strength compared to other materials, meaning that it is light weight while it can withstand immense force (Förlich et al., 2019). Thus, by understanding how diatoms construct the frustule one can get insight into how to make materials with the same qualities. The frustule also has an intricate pattern that is highly conserved between generations, and is specific for each species. It is therefore believed that many genes are involved in the process (Falciatore and Bowler, 2002).

1.2 Frustule structure and formation

The features of the diatom frustule affect many of the different factors essential for survival, such as uptake of nutrients (Finkel and Kotrc, 2010), sinking rate (Raven and Waite, 2004), exposure to predators (Hamm et al., 2003), resistance against viral attacks (Losic et al., 2006) and light perception (Fuhrmann-Lieker et al., 2004). The frustule consists of two identical halves, the two thecas, where one is slightly bigger than the other. This causes an overlap where they meet, such as a on a petri dish. The surface at each end is called the valve and the side is called the cingulum, which consists of several bands called the girdle bands. The bands that are in the region of overlap between the two thecas are called the pleural bands (Figure 1.1) (Falciatore and Bowler, 2002). Diatoms can be sorted into two groups based on their structural symmetry; centrics, which are radially symmetrical, and pennates, which are bilaterally symmetrical. For the centrics, *Thalassiosira pseudonana* (*T. pseudonana*) is most often used as a model organism. This species is used because it has a small genome, which has been sequenced (Armbrust et al., 2004). In addition, the species has not been observed to reproduce sexually, which makes cultivation of the cells less complicated.

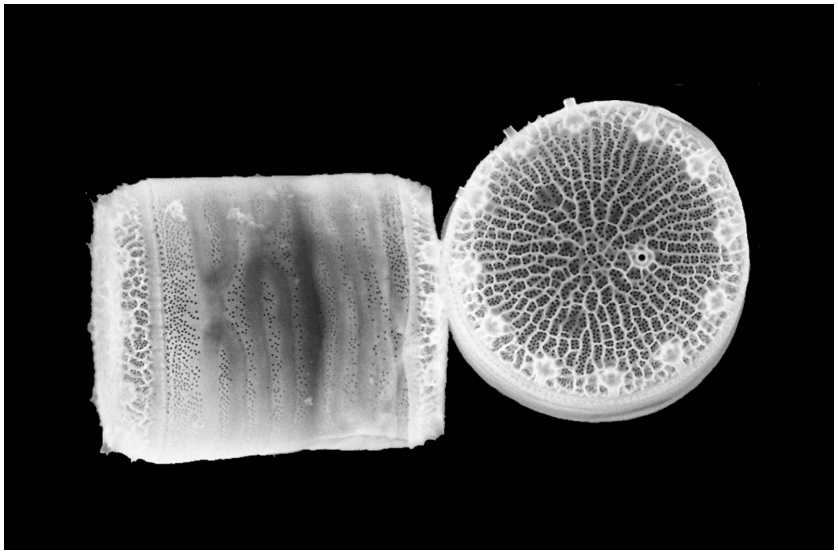

Figure 1.1: An electron microscope image of two cells of *T. pseudonana*. The cingulum and girdle bands are seen on the left cell, while the valve, is seen on the right (N. Kröger).

This is not the case for most other diatom species, as they usually get smaller each generation of cell division. Thus they need to reproduce sexually every few generations in order to get back to their full size. It is not known how *T. pseudonana* avoids this, but it is thought to be due to a mechanism that makes the valve expand outside of cell (Kröger and Poulsen, 2008). The valve of the frustule of *T. pseudonana* has been shown to have a distinct pattern (Figure 1.1). In the centre of the valve is the pattern centre, which is the site where valve formation is initiated. Radiating from the centre are ribs, which are regularly spaced and branched towards the rim. The ribs are connected through cross-connections. In addition, small nanopores are interspaced between the ribs, and larger pores called rimoportulae are found at the rim of the valve. Usually, a similar pore called the fultoportula is also found offset from the centre of the valve (Hildebrand et al., 2006). The overall structure of the frustule can be divided into 3 scales: nanoscale, mesoscale and microscale. The nanoscale structure are the structures of less than 40 nm, and covers the initial Si-polymerisation. The mesoscale structures are assemblies of nanoscale blocks, and includes structures such as the ribs and rimoportulae. The microscale structures are the overall three-dimentional shape of the frustule (Tesson and Hildebrand, 2010b).

When a diatom cell divides, the two daughter cells first stay within the frustule of the mother cell (Figure 1.2). Both cells begin producing a

new valve in a membrane-bound organelle called the silica deposition vesicle (SDV). Here, the base layer is the first part of the frustule to be formed. This will be the surface of the finished valve that is proximal to the cell (Kröger and Poulsen, 2008). The pattern of the finished valve is decided by the base layer, which is decided by the features of an organic matrix. The matrix contains a durable layer of proteins called the Ammonium Fluoride insoluble matrix (AFIM), which is named so because of its insolubility when treated with ammonium fluoride (Hildebrand et al., 2018). As the valve expands, the SDV expands with it, until it reaches its full size. Then, the complete

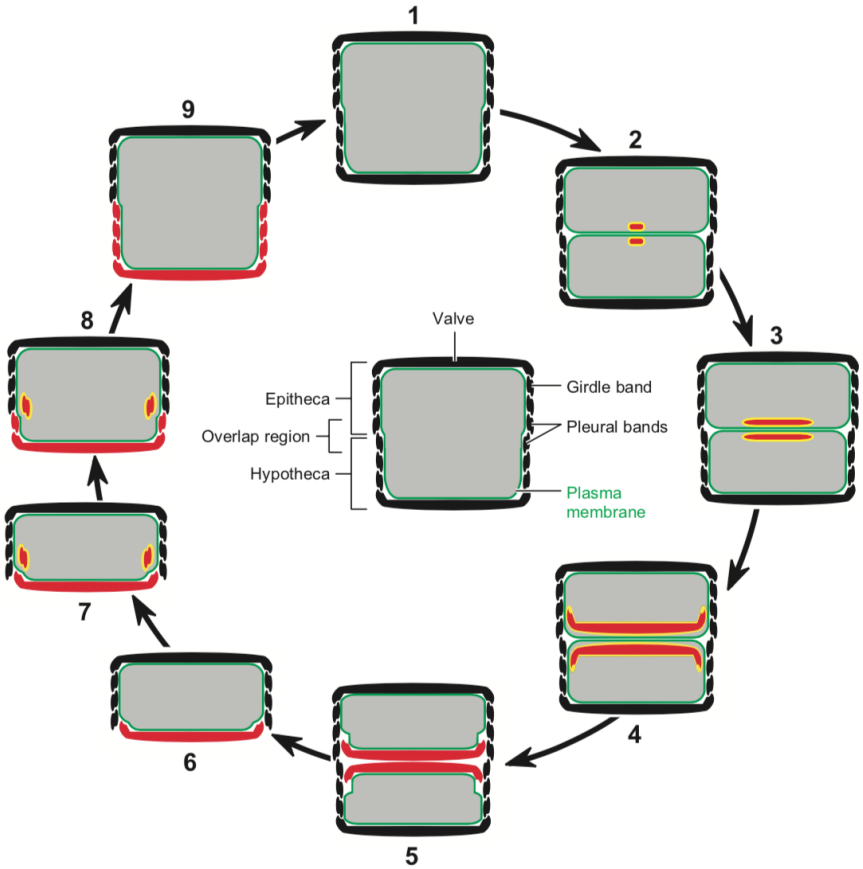

Figure 1.2: The cell cycle of diatoms. (1) A full size diatom cell. (2) The mother cell divides into two daughter cells. The SDV of each cell (yellow) starts producing a new valve (red). (3) The SDV expands with the valve, until (4) the valve is of full size. (5) The cell exocytoses the valve, and (6) the daughter cells separate completely. (7+8) the SDVs produce new girdle bands (red), elongating the cell until (9) the cell is of full size (Kröger and Poulsen, 2008).

valve is exocytosed, and the two daughter cells separate. The cells are now half the length of the original mother cell, thus they begin producing girdle bands in new SDVs. The bands are produced and exocytosed until the cell again reaches its full length (Kröger and Poulsen, 2008).

1.3 Silicanins

As research tries to find out how the frustule is synthesised, there have been done functional studies on the proteins that are suspected to take part in the process. An article published by Kotzsch et al. (2016) did a proteomics analysis of the AFIM found in *T. pseudonana* and found several proteins, one of which later has been known as Silicanin-1 (Sin-1). Because it did not show any similarity to known frustule-forming proteins it was thought to belong to a novel family of genes (Kotzsch et al., 2016). In experiments by Brembu et al. (2017), a group of genes that showed structural similarity to *Sin-1* was discovered. This new family was called the silicanins. 15 silicanins were found in *T. pseudonana* and 10 were found in *Phaeodactylum tricornutum* (*P. tricornutum*). The two species are distantly related, which suggests that the genes are conserved well within diatoms. The silicanins can be divided into 4 sub-families, where all are present in both *T. pseudonana* and *P. tricornutum*. The silicanins all have a similar domain composition, with a signal peptide for co-translational transport into the endoplasmic reticulum (ER), an RXL protease cleavage site, a region with 8 conserved cysteines, and a transmembrane domain (Figure 1.3). Because of the transmembrane domain, the silicanins are thought to go through the SDV membrane, also called the silicalemma (Brembu et al., 2017).

Figure 1.3: Predicted domain structure for the Silicanins. SP, signal peptide; RXL, protease cleavage motif; TM, transmembrane domain (Brembu et al., 2017).

Knock-out experiments of Sin-1 in *T. pseudonana* has been shown to yield less prominent cross-links in the valve. It is very likely that cross-connections, and thus Sin-1, contribute to the high specific strength of the frustule. This was further investigated by indenting the frustule with a sharp tool, and seeing how it would affect the cell, and specifically the frustule. The knock-out mutants' frustule caved at a relatively low pressure compared to

the wild-type, which indicated a reduced mechanical strength and stiffness (Förlich et al., 2019).

The silicanin Tp24711 discovered in Brembu et al. (2017) was studied further by Gresseth (2019). The thesis suggested that the gene was involved in production of both valve and girdle bands, as a fluorescent fusion gene of the protein was found located in these regions. The expression of the gene was upregulated in the G2 and M stages of the cell cycle, which could confirm an involvement in frustule formation during cell division.

It has been hypothesised that the cytoskeleton of diatoms takes part in formation of the frustule, but in order for that to happen the cytoskeletal networks would have to communicate with the inside of the SDV. It has therefore been concluded that some transmembrane proteins are involved in communicating between the cytoskeleton and the frustule (Hildebrand et al., 2018). As Tp24711 and the rest of the protein family are thought to cross the silicalemma it is speculated that they could be this connection between the cytoskeleton and the SDV lumen (Brembu et al., 2017).

1.4 The cytoskeleton

1.4.1 Microtubules

Among the types of cytoskeletal networks in eukaryotic cells, you find a polymer called the microtubules. The microtubules are built up of heterodimers consisting of α- and β-tubulin, which are two proteins with a similar structure (Figure 1.4). In the microtubules, these are organised in a such a way that they make up a long, hollow tube. The tubulins are able to bind to GTP, which is required in order for the dimers to polymerise. After polymerisation, the GTP is hydrolysed and transformed to GDP. This is a less stable form, and is more prone to depolymerise than GTP-bound tubulins. It takes some time for GTP to be hydrolysed. Therefore it stays on the end of the microtubules as a protective cap after polymerisation. If the microtubules go too long without adding new tubulins, all the GTP is hydrolysed and the protective cap is gone. The GDP-bound tubulins will then rapidly depolymerise, and the microtubules shrink until new GTP-tubulins are bound to make a new cap (Hardin et al., 2017).

The microtubules have many cellular functions, such as intracellular transport and chromosomal movement (Hardin et al., 2017). In diatoms, the microtubules have been found to control the shape of the SDV, which may take part in formation of the frustule on a microscale and contributes to maintaining the tension of the SDV. Osmotic pressure could lead to structural deformations of the silica, so the microtubules may minimise the structural impact.

In addition, it is thought that the microtubules aids in positioning the newly synthesized valve (Tesson and Hildebrand, 2010b). Experiments introducing microtubule inhibitors in the diatom *Cyclotella cryptica* (*C. cryptica*) have also shown that microtubules may also be involved in positioning of the fultoportulae and alignment of the ribs (Tesson and Hildebrand, 2010a).

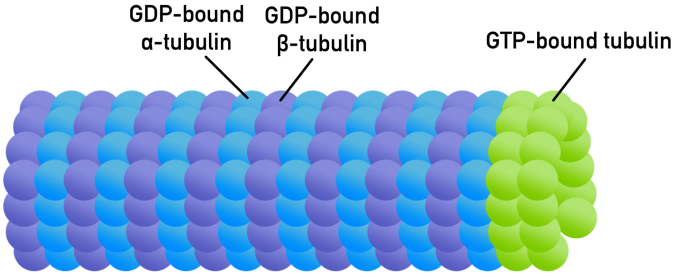

Figure 1.4: Schematic representation of a microtubule strand. The α- (blue) and β-tubulin (purple) form dimers oriented next to each other in a tubular shape. On the end of the strand are tubulins bound to GTP (green), which form a protective cap that prevents the microtubule from depolymerising rapidly. Adapted from Hardin et al. (2017)

Some drugs can be used to disrupt normal microtubule formation, such as colchicine and oryzalin. Colchicine works by binding to β-tubulin, thereby inhibiting incorporation of new heterodimers onto the microtubules. This further inhibits formation of a new GTP-cap and therefore destabilise the structure, promoting microtubule disassembly (Hardin et al., 2017). Oryzalin, on the other hand, works by binding to α-tubulin, thereby disrupting binding to adjacent heterodimers. The two inhibitors are believed to affect the microtubules in similar ways (Morrissette et al., 2004).

1.4.2 Microfilaments

Microfilaments are another type of cytoskeleton. They are built up of two strands of actin proteins, which are coiled around each other (Figure 1.5). The actin proteins are all oriented in the same direction, giving the filaments polarity. The two poles differ in that new actin monomers are more rapidly added to the plus end than the minus end. If there is little silica in the medium, however, the strands depolymerise more rapidly on the minus end than the plus end. Cytochalasin D is an effective drug for inhibiting the polymerisation of actin. It works by capping the plus end of the filaments,

making new actin unable to be incorporated on the filament. However, the minus end is still open, making the strands keep depolymerising. The actin strands then shrink, and are thus unable to perform their cellular functions (Hardin et al., 2017).

In general, microfilaments are responsible for different cellular functions such as cell shape and effective cytokinesis (Hardin et al., 2017). In diatoms, microfilaments have also been found in association with both the girdle bands and the valve while they are produced in the SDV. Two rings have been seen in valve formation, where the outer ring defines what will be the rim of the finished valve, while the inner ring is associated with the edge of the SDV during silification. It is thought that the actin is involved in silification on a microscale by shaping the SDV, thereby affecting the shape of the valve (Tesson and Hildebrand, 2010a). In addition, actin is thought to take part in frustule formation on mesoscale. A close interaction between the actin filaments and the silica structures have been observed *in vivo* in several species. It has therefore been suggested to be involved in several structures such as ribs (*C. cryptica*), fibulae (*Nitzshia curvilineata*) and the raphe (*Entomoneis alata*) (Tesson and Hildebrand, 2010b). In addition, experiments using microfilament inhibitors in the diatom *C. cryptica* affected the growth of silica around the fultoportulae, resulting in open slits in stead of the circular shape observed in normal frustules. The regions of nanopores were also affected, as they weren't raised above the valve, like they usually are (Tesson and Hildebrand, 2010a). It has been hypothesised that the microfilaments may use silicalemma-spanning proteins to take part in mesoscale assembly through the silicalemma (Robinson and Sullivan, 1987), although these proteins have not yet been identified.

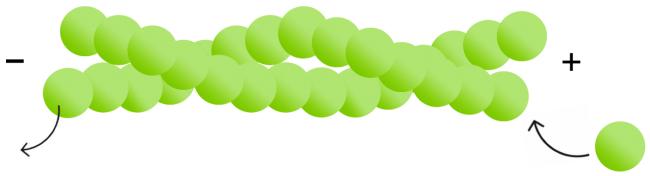

Figure 1.5: Schematic representation of microfilaments. Two strands consisting of adjacent actin proteins are twisted around each other. New actin proteins are added to the positive end, and old proteins are removed from the negative end. Adapted from Hardin et al. (2017)

1.5 The role of diatoms in future technology

In the most recent decades, there has been an increasing interest in understanding the mechanism of diatom frustule formation. This is due to the many applications of mesoporous silica, and the advantages of a biomimetic formation of it. Previously, it has been common to make silica structures chemically, which requires harsh reaction conditions and complicated approaches of synthesis (Lechner and Becker, 2015). In addition, these methods do not provide silica that has the same level of intricacy as the biologically synthesised.

The production of MCM-41, a chemically synthesised silica material, was a breakthrough in biotechnological applications in 1992. It became possible to obtain a ordered mesoporous silica-based material, which could be easily altered by changing simple parameters such as silica source, surfactant, pH and temperature (Wan and Zhao, 2007). This material could be used in multiple applications, for example as a stationary phase in HPLC, filling material and a way of drug distribution. By modifying the surface of mesoporous silica particles, the drugs adsorbed to the particles could be targeted to specific parts of the body, and release drugs in a targeted matter. In addition, premature release of the drugs was avoided by using pH-dependent, redox responsive or enzymatic gatekeepers. These gate-keepers were removed when exposed to a different pH, reducing molecules or specific enzymes, respectively. When they were removed the drugs were released in a continuous matter. Using mesoporous silica particles for this, less drugs were needed per treatment and only the desired cells of the body were exposed (Lechner and Becker, 2015).

Remains of diatoms found on the ocean floor has also been utilised, although for other applications than the man-made silica. These remains are called diatomaceous earth, and consist mainly of the remnants of old diatom frustules. An unfortunate disadvantage of diatomaceous earth is that it has been exposed to the environment for millions of years, and therefore lacks the desired morphological features, such as the intricate pores, that are seen in newly synthesised frustules (Vrieling et al., 1999). By being able to replicate the natural process of silica polymerisation in diatoms, one can get siica formations with the same characteristics as in frustules, or even silica particles with structures tailored to the needs of the producer. Understanding how the intricate diatom cell wall is made could also lead to simpler pathways of synthesis of the desired materials, and more detailed structures that are made chemically today.

1.6 Aim of the thesis

Knowledge about the many frustule-producing proteins of the diatoms could yield insight in making complex materials. The more that is known about the elaborate synthesis pathway, the better the materials can become. Research on the Tp24711 protein could be a small part of the bigger picture in this advancement. Intracellular locations of the protein were identified in Gresseth (2019), by making mNeonGreen-Tp24711 transformants. These transformants were going to be used for further investigation, but lost their mNeonGreen fluorescence. The aim of this thesis is to investigate what happened to the fluorescence of the mNeonGreen-Tp24711 transformants, in addition to characterising the effect cytoskeleton inhibitors have on frustule morphology. The thesis also aims to give an overview over existing research on proteins and organic molecules involved in frustule synthesis.

2 Materials and methods

Because of the COVID-19 pandemic access to the lab was restricted, which lead to some parts of the experiments being performed by other individuals. This includes picking of colonies after transformation, which was done by Marthe Hafskjold, and determination of the most fluorescent clones, which was done by Annika Messemer. The confocal microscopy was performed by Tore Brembu, and the SEM was performed by Thi My Linh Hoang.

2.1 Diatom culture conditions

T. pseudonana of the CCMP1335 strain from The Culture Collection of Algae and Protozoa were used for the thesis. The cells were grown in f/2 medium (see Appendix A.1) at 18 °C under continuous light.

2.2 Production of mNeonGreen-Tp24711 transformants

A mNeonGreen-Tp24711 fusion gene was utilised to locate the Tp24711 protein product inside *T. pseudonana*. Two transformants of a pTpPuc3-plasmid containing this insert were initially prepared in Gresseth (2019), named the Tp24711-1.2 and Tp24711-1.5 transformants. At some point, these cells lost their ability to express mNeonGreen fluorescence, which will be shown and discussed in further detail in Sections 4 and 5. These transformants were called the first generation. User solutions of the pTpPuc3 plasmid containing the mNeonGreen-Tp24711 fusion gene prepared in Gresseth (2019) had been retained and could be used again in a new transformation following the same protocol. The plasmid is illustrated in Figure 2.1, and contains selection markers that confer resistance against kanamycin (kan) in *Escherichia coli* (*E. coli*) and nourseothricin (nou) in *T. pseudonana*.

2.2.1 Transformation of plasmid into *E. coli*

To introduce the plasmid into *T. pseudonana*, the protocol described in Karas et al. (2015) was used. First, the plasmid was introduced to DH10B-*E. coli* cells by heat-shock transformation. These cells had already been transformed with a plasmid that makes them able to conjugate, called pTa-Mob (Strand et al., 2014). The plasmid contains a selection marker that confers resistance againt gentamycin (gent).

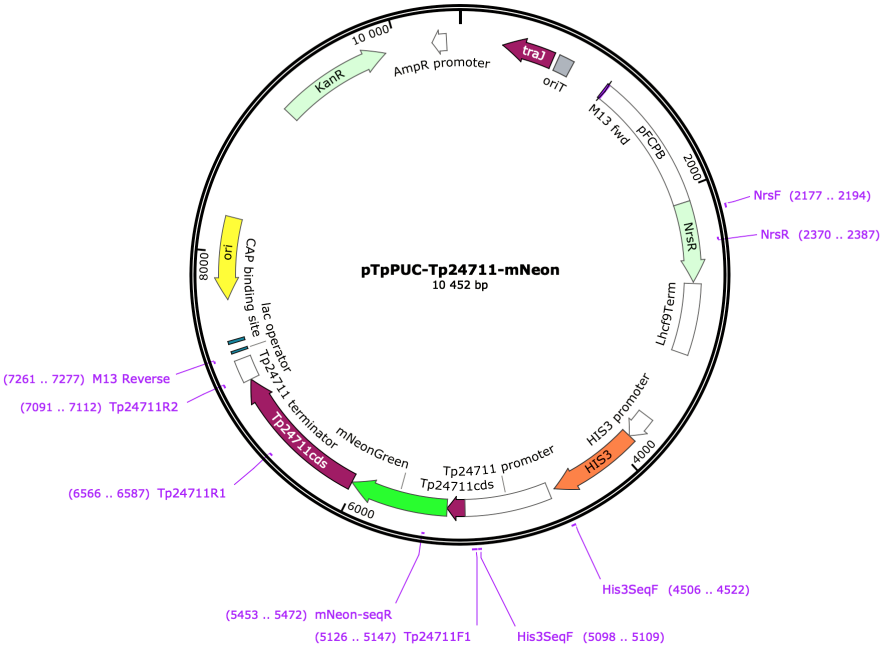

Figure 2.1: The pTpPuc3 plasmid with the mNeonGreen-Tp24711 fusion gene insert. The features of the plasmid are denoted with arrows, and some of the relevant primers are denoted in purple.

1 µl of the plasmid was added to 100 µl of the cells. This was mixed carefully and incubated on ice for 30 minutes. The cells were heat-shocked by incubating at 42 °C for 45 seconds and then moved to ice for 2 minutes. 2 ml of pre-warmed 37 °C LB medium (see Appendix A.2) was added to the tube, and it was again incubated at 37 °C for 1 hour, with shaking at 220 rpm in a Multritron incubation shaker from INFORS HT. 100 µl of the mix was added to pre-warmed LB plates (37 °C) with 50 mM kan and 10 mM gent. This was incubated overnight at 37 °C. The next day, a colony was picked and placed in a tube containing 20 ml of LB medium with 50 mM kan and 10 mM gent. The culture was incubated overnight at 37 °C and shaking at 220 rpm.

2.2.2 Conjugation of plasmid into *T. pseudonana*

The optical density (OD) of the *E. coli* culture was measured, and the culture was diluted to reach an approximate value of 0.1. The culture was grown at 37 °C and agitation at 220 rpm. The OD was measured every hour, until it reached 0.3. The culture was spun down at 5 500 g for 10 minutes and resuspended in 800 µl of SOC media (see Appendix A.3). Wild-type cells

of *T. pseudonana* were spun down at 5 500 g and 10 °C for 10 minutes, and resuspended in L1 medium (see Appendix A.4) to reach a final concentration of approximately $2 \cdot 10^8$ cells per ml. 200 µl of the transformed *E. coli* culture and 200 µl of wild-type *T. pseudonana* culture were mixed gently, and 200 µl was plated on 1/2 x L1 plates containing 5 % LB medium. The plates were incubated in the dark for 90 minutes at 30 °C, and then in light at 18 °C for 4 hours. 1 ml of L1 medium was added to the plates, and the cells were scraped off. 200 µl of the resulting cell cultures were added to new plates containing 1/2 x L1 with 50 mM nou. The plates were incubated at 18 °C and constant light until colonies appeared on the plates. Several colonies were picked 16 days after plating, and cultivated in wells containing f/2 medium. The new transformants will henceforth be called the second generation. The clones were cultivated in wells for 34 days before the two most fluorescent clones were decided by flow cytometry (see Section 4.1). These two were chosen to be cultivated for further experiments, and were named were named the Tp24711-2.4 and Tp24711-2.9 transformants.

A third generation of transformants were made by picking colonies from the same plate as the second generation and incubating them in f/2 medium with 50 mM nou. These plates were stored at 4 °C after the second generation of transformants was picked. After incubation the most fluorescent clone was decided by flow cytometry (see Section 4.1), and the Tp24711-3.11 transformant was chosen for further studies.

2.3 Inspection of transformants

The mNeonGreen-Tp24711 transformants were studied using fluorescence microscopy, confocal microscopy and flow cytometry.

2.3.1 Fluorescence microscope

The fluorescence microscope is a Zeiss Axio Imager.Z2 microscope with a 40x Plan Apochromat objective. This used an HXP-120 UV light source. The microscope had a 505-555 nm emission filter to detect mNeonGreen fluorescence, and a >650 nm emission filter to detect autofluorescence emitted from the chloroplasts. Several of the fluorescent images showed only a weak fluorescence, and the colour contrast was therefore increased in order to illustrate the location of the fluorescence better.

2.3.2 Confocal microscope

The confocal microscope used was a Leica TCS SP5 with a 63x water objective. This used a 488 nm laser (30 %), and detected fluorescence between 500-570 nm, which should be in the range of mNeonGreen fluorescence. In addition, it had a > 650 nm emission filter, which gave an indication of the autofluorescence. Several of the fluorescent images showed only a weak fluorescence, and the colour contrast was therefore increased in order to illustrate the location of the fluorescence better.

2.3.3 Flow cytometer

The flow cytometer was a BD Accuri^{TM} C6 Plus Flow Cytometer with a Fl1 (533 ± 15 nm) and Fl3 (670 nm LP) emission detector, and a 488 nm laser. The flow cytometer was set to count 5 000 events (cells). Fluorescence and Forward scatter (Fsc) was measured for each of the events. The fluorescence is measured by estimating the number of fluorescent particles per event, and the Fsc indicates the size of the event by measuring the amount of light that passes by the event. The concentration of the culture can be estimated by dividing the number of events counted by the amount of media used. Some of these events may be dead cells or cell debris, which is why these events were removed by gating only the cells with high Fl3-fluorescence (above approximately 50 000 fluorescence units (fu)).

2.4 Synchronisation experiments

2.4.1 Starvation of silica

To synchronise the cells in each culture, 3 ml of Tp24711-1.2, Tp24711-1.5 and wildtype culture was added to 27 ml of f/2 medium without SiO_2 and nou selection. The resulting cultures were incubated at 18 °C, constant light and shaking at 120 rpm on a MaxQ 2000 open-air platform shaker from Thermo Scientific, while the cell density was monitored through a flow cytometer. The synchronisation experiment was done three times. In the first and second experiment the cultures were starved for 24 hours. The cell density was adjusted in the second experiment in order for the cultures to reach an approximate density of $1 \cdot 10^6$ cells per ml before addition of silica. This density has been shown to be suitable in previous experiments by Hildebrand et al. (2007). In the third experiment the cultures were starved for 48 hours, with 4 measurements at even intervals to see if the cultures had in fact halted their growth. In addition, the cell density was adjusted such as described for the second experiment.

2.4.2 Replenishment of silica

After the starvation period Na_2SiO_3 was added to the cultures to a final concentration of 300 µM. Samples were taken from the cultures and analysed on the flow cytometer before Si-addition, and once or twice every hour after addition. The flow cytometer counted 10 000 events for each sample. The experiment was run until the results seemed to be sufficient to draw conclusions about mNeonGreen expression during the cell cycle. The experiment length thus differed for each of the experiments.

2.4.3 Cell stage determination

Additional samples of 2.5 ml were taken during the third experiment, which were used to determine which part of the cell cycle the cells in the cultures were in. These samples were treated based on a process described by Traller and Hildebrand (2013), in order to colour the DNA of the cells. The samples were spun down at 5 000 g for 7 minutes and the supernatant was removed. The cells were resuspended in 1 ml of 100 % ice-cold methanol, and stored at 4 °C for 24 hours. The samples were spun down again, and resuspended in 1 ml of Trisaminomethane (Tris)-Ethylenediaminetetraacetic acid (EDTA) buffer (pH 8). This was repeated twice. The cells were then resuspended in 1 ml Tris-EDTA, and DNAase-free RNAase was added to a final concentration of 0.3 mg/ml. This was then incubated for 60 minutes at 37 °C. Afterwards, 10 µl of 100X SYBR green (dissolved in Dimethyl sulfoxide (DMSO)) was added to each of the samples, and they were incubated on ice for 10 minutes in the dark. SYBR green fluoresces when it binds to the double-stranded DNA of the cell. Each of the samples were analysed on a flow cytometer. This time, an ACEA Novocyte® flow cytometer was used, with BL1 (530 ± 15 nm) and BL4 (675 ± 15 nm) emission filters. The ACEA Novocyte® had a software called NovoExpress®, which was able to recognise in which phase of the cell cycle each cell was based on the fluorescence intensity, and thereby the amount of DNA in the cells. This was done by analysing the amount of fluorescence emitted from each of the cells, in the range of SYBR greeen (Bl1). The cell cycle is parted into three, based on the DNA content of each part (Figure 2.2). The G2 and M phase of the cell cycle should contain twice as much DNA as the G1 phase, yielding a stronger fluorescence. The cells in the S phase should be somewhere in between.

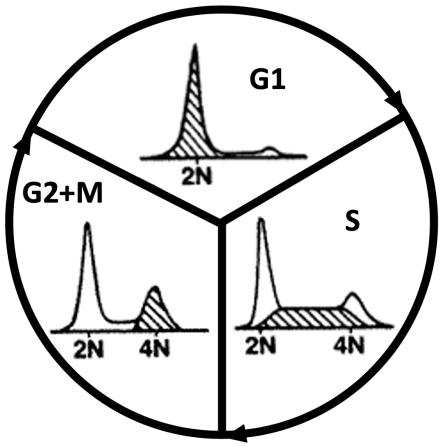

Figure 2.2: A representation of the cell cycle. The graphs are representations of the output of the cell cycle determination software, where the amount of cells is plotted as a function of fluorescence intensity. Each cell stage is represented in its own part of the graph, as illustrated by the shaded area under the curve. Adapted from Rabinovitch (1993).

2.5 Western blotting

2.5.1 Protein isolation

A western blot was done to identify whether the first generation of transformants expressed mNeonGreen. First, protein isolation was done on the Tp24711-1.2 and Tp24711-1.5 transformants in addition to a wild-type negative control culture. The samples were taken from the third synchronisation experiment at 4 hours after Si-addition. The process was done according to the protocol described in Nymark et al. (2019). The cells were harvested from the culture using vacuum filtration with a Durapore 0.65 µm PVDF filter (Millipore). The filters were transferred to 2 ml tubes containing 1 ml of f/2 medium. The cells on the filter were resuspended by vortexing for approximately 10 seconds, after which the filters were removed. The tubes were centrifuged for 1 minute at 16 000 g and 15 °C. The supernatant was removed, and the pelleted cells were frozen in liquid nitrogen and put in a -80 °C adapter for TissueLyser. One 5-mm cooled stainless-steel bead was added to each of the tubes, and the adapter was shaken in the TissueLyser from Qiagen at 25 Hz for 2 minutes. The tubes were moved to a room-tempered adapter set and 700 µl of lysis buffer was added. This buffer consists of 50 mM Tris and 2 % SDS at pH 6.8. The adapter was shaken again for 8 minutes at 25 Hz. The tubes were centrifuged for 30 minutes at 130 g and 4

°C, and the supernatants were transferred to 1.5 ml tubes, while the pellets were discarded. The protein concentration was determined using a Qubit from Thermo Fisher Scientific (see Appendix B).

DH5α *E. coli* cells transformed with a pNCS-mNeonGreen plasmid was used as a positive control for the blot. The mNeonGreen-protein had been pre-isolated from the cell culture.

2.5.2 SDS-PAGE

After the proteins were isolated, the samples were separated using Sodium dodecyl sulfate (SDS)-PAGE. 5 µl of NuPAGE™ LDS sample buffer (4X) from Invitrogen™ was added to 15 µl of sample. This was heated at 50 °C for 30 minutes and pipetted equally into the wells of two SDS-PAGE gels (Appendix C.1) as seen in Table 2.1. In addition to analysing the untreated cultures, one of the transformants and the positive control were pelleted by centrifugation of 100 µl culture at 6 500 g for 10 minutes.

Table 2.1: The samples that were run on SDS-PAGE. Some of the samples were run several times; as culture, as pellet or as supernatant from pelleted culture. The pellets were diluted using MQ to obtain a total volume of 15 µl of sample in each well.

Sample [µl]	Content	MQ [µl]
5 µl	mNeonGreen-producing *E. coli*	10 µl
Pellet	Pelleted mNeonGreen-producing *E. coli*	15 µl
15 µl	Tp-WT	
15 µl	Tp24711-2 transformants	
15 µl	Tp24711-5 transformants	
15 µl	Supernatant from pelleted Tp24711-2 transformants	
Pellet	Pellet from pelleted Tp24711-2 transformants	15 µl

One of the gels was rinsed 3 times for 5 minutes in Milli-Q® (MQ) water. The gel was then incubated in 20 ml of SimplyBlue™ SafeStain from Invitrogen™ for 1 hour under agitation, and rinsed again in 100 ml of MQ for 3 hours under agitation. This should yield an image of the total protein content in the cells.

2.5.3 Western blot

A PVDF membrane was equilibrated in 100 % methanol for 30 seconds, and then washed in MQ for 2 minutes. The membrane was then equilibrated

in Twobin buffer for 10 minutes with agitation, and the other gel was equilibrated in Twobin buffer for 10 minutes. Filter paper, gel, membrane and a new filter paper was stacked on top of each other and rolled over to remove air bubbles. This was blotted for 30 minutes at 25 V and 1 A in a Trans-Blot® Turbo™ transfer system from Bio-Rad. The membrane was pre-activated with 100 % methanol, and then rinsed with MQ. It was then immersed in 5 ml of iBind solution (see Appendix C.2). The membrane was put into the iBind™ Flex Western Device from Thermo Fisher Scientific, and air bubbles were removed. The device contains four wells, which were loaded with 2 ml primary antibody (mNeonGreen tag Rabbit AB from Cell Signaling Technology®), 2 ml 1X iBind solution, 2 ml secondary antibody (Goat anti-Rabbit IgG (H+L), peroxidase conjugated from Invitrogen™) and 6 ml of 1X iBind solution. This was incubated until all the wells were empty (2.5 hours), and the membrane was taken out and rinsed with 20 ml of MQ for 2 minutes. The blot was then incubated for 5 minutes in SuperSignal West Pico PLUS Chemiluminescent working solution (50 % Luminol/Enhancer, 50 % peroxide) from Thermo Fisher Scientific. The excess reagent was drained, the blot was wrapped in plastic wrap and the air bubbles were removed. The blot was imaged in a ChemiDoc XRS+ System from Bio-Rad.

2.6 Analysis of non-fluorescent transformants

mNeonGreen-Tp24711 transformants from two transformations, where the second transformation plate was picked twice, were studied in this thesis. As all three generations lost their ability to express mNeonGreen fluorescence at some point, some of these clones were investigated further through PCR and gel electrophoresis. The second generation of transformants were chosen for this. Four fragments were amplified from both clones, and one wild-type culture was used in addition for reference.

In order to isolate DNA from the transformants cells were extracted from 40 ml culture by filtering using a vacuum pump onto a Durapore 0.65 µm PVDF filter from Millipore. The filters were transferred to 2 ml tubes containing 1 ml of f/2 medium. The cells on the filter were resuspended by vortexing for approximately 10 seconds, after which the filters were removed. Afterwards, the protocol from the DNeasy Plant Pro kit from Qiagen was followed (see Appendix C.3). After the DNA had been extracted from the cells, a 50 µl PCR reaction using the Phusion® High-Fidelity DNA polymerase from New England Biolabs® was run. The details of the PCR are given in Appendix C.4. The amplified segments are represented in Table 2.2 and their primers are illustrated in Figure 2.1. The PCR products were separated using gel electrophoresis on a 1 % agarose gel with GelRed for

staining.

Table 2.2: The primers used for PCR of the the second generation of non-fluorescent mNeonGreen-Tp24711 transformants.

Primer forward	Primer reverse	Length of fragment
His3seqF	mNeon-seqR	967
His3seqF	M13 Rev	2 772 bp
Tp24711-F1	Tp24711-R1	1 462 bp
Tp24711-F1	Tp24711-R2	1 987 bp

2.7 Titration of cytoskeleton inhibitors

Two microtubule inhibitors (colchicine and oryzalin) and one actin inhibitor (cytochalasin D) were used for the experiments. In order to investigate the effect of these inhibitors on frustule biosynthesis, the growth of the cells should be inhibited but not stopped. To find the ideal concentration of each inhibitor 4 different concentrations was used on the two transgene lines and on the wildtype (Table 2.3). They were made from stock solutions of 3 mM cytochalasin D (dissolved in DMSO), 50 mM colchicine (dissolved in water) and 2 mM oryzalin (dissolved in water).

Table 2.3: The concentrations that were used to find a suitable inhibition concentration of each inhibitor. The concentrations denoted in bold were ones that have previously been used in experiments done by Tesson and Hildebrand (2010a) on *C. cryptica*.

Cytochalasin D:	1.5 µM	**3 µM**	6 µM	12 µM
Colchicine:	25 µM	**50 µM**	100 µM	200 µM
Oryzalin:	0.1 µM	**0.2 µM**	0.4 µM	0.8 µM

In addition, a wildtype culture was grown without addition of inhibitor, in order to have a reference point for growth. The cell concentration of the cultures were measured before addition of inhibitor, and 48 hours after. The flow cytometer measured 5 000 events (cells).

2.8 Effect of cytoskoskeleton inhibitors on frustule morphogenesis

The effect of the different inhibitors on frustule morphogenesis was investigated by studying inhibitor-affected frustules through Scanning Electron Microscopy (SEM). Three 50 ml cultures of wild-type *T. pseudonana* were set up with oryzalin (0.2 µM), cytochalasin D (6 µM) and colchicine (40 µM), and one culture was cultivated without any addition of inhibitors. The cultures were incubated for 4 days. The cells were centrifuged at 3 700 g for 10 minutes. In order for the frustules of the cells to be observed they first had to be thoroughly cleaned, which was done according to the "soft" protocol described in Romann et al. (2016). The cells were washed 3 times using 25 ml MQ, and spun down at 3 700 g for 10 minutes at each wash. The supernatants were removed carefully, and the pellets were dried overnight at 60 °C. 4 ml of a solution of 5 % SDS and 100 mM EDTA at pH 5 was added to the dried cells, and vortexed for 1 minute, left still for 20 minutes, and centrifuged at 3 700 g for 10 minutes. The process was then repeated 6 times, and in the end the material was washed three times with MQ and centrifuged at 3 700 g for 10 minutes. The frustules were still visibly contaminated by organic material, and the same cleaning step with SDS/EDTA were repeated 4 more times. After the last iteration the frustules were washed three more times with MQ water, resuspended in 1 ml 96 % ethanol, and stored at 4 °C.

The cleaned frustules were imaged using SEM. Here, the samples were centrifuged carefully until the frustules were pelleted. The ethanol was removed by pipetting, leaving only approximately 300 µl. The pellet was resuspended in the remaining ethanol through vortexing. A double-sided carbon tape was fastened to the SEM pin, 10x10 mm slides of Silicone were added to the tape, and all dust was blown off. 15 µl of the sample was pipetted onto the slide, and it was air-dried for 30 minutes. Gold was sputtered on in a thickness of approximately 15 nm, and the slides were imaged in a Teneo SEM from Thermo Fisher Scientific. It was set to HT at 10 kV, a beam current of 0.1 nA and at high-vacuum mode. An Everhart-Thornley Detector was used, and the magnification was at 20 000x. The valves of the cells were the main focus of the imaging.

2.9 Literature review

The literature review was performed by searching in Oria, which is the NTNU library's electronic collection of books, articles, etc. The search mainly included the name of the protein or molecule in question with "diatom" behind. The result of the search differed for each molecule, as the

existing research had focused on different methods. The review is still focused on primarily structure and function. There was also a difference in quantity of articles, as some molecules were more explored than others.

3 Literature review: Proteins and organic molecules involved in frustule synthesis

The most explored proteins and organic molecules involved in frustule formation will be described in the following sections. The silicanins were not included, as they have been described in detail in Section 1.3. In the end, some proteins that are not involved in frustule synthesis, but are still involved in frustule functionality will be described.

3.1 Silaffins

Silaffins are a family of proteins that were discovered from extracts of hydrogen fluoride-treated frustules. They are named silaffins because of their great affinity for silica. Initially, 3 different silaffins were identified in *Cylindrotheca fusiformis* (*C. fusiformis*) at three different molecular weights; Silaffin-1A (Sil-1A, 4 kDa), Silaffin-1B (Sil-1B, 8 kDa) and Silaffin-2 (Sil-2, 17 kDa). Sil-1A and Sil-1B was discovered to originate from the same precursor protein, Silaffin-1P (Sil-1P), and is subjected to proteolytic cleavage during maturation. The Sil-1P protein has a N-terminal that provides a signalling sequence for co-translational transport into the ER. In the middle is a long domain that, thus far, has an unknown function. The C-terminal has seven similar consecutive sequences (R1-R7) that give rise to the different mature Sil-1 proteins (Figure 3.1). The end of each repetitive sequence contains a RXL cleavage site, which is targeted by a endoprotease in order to give rise to seven mature proteins. The mature proteins containing sequences R2-R7 are Sil-1A proteins, while the protein containing R1 is the bigger Sil-1B. What is so distinctive about the repetitive sequences is that they contain a high amount of the amino acids lysine and serine (Kröger et al., 1999). These amino acids go through post-translational modifications (PTMs), which make the mature proteins become large zwitterions. In Sil-1A, for instance, N-methylated oligo-propyleneimine chains are covalantly attached to the lysine residues, and the serine residues are phosphorylated. Another feature that seems to be present in most silaffins is that the lysine elements are often gathered in KXXK sequences, where K is lysine and X can be a variety of amino acids. It has been suggested that this KXXK motif is a recognition site for PTMs (Kröger et al., 2002). Other diatom species have also been known to produce silaffins, although the sequence does not seem to be conserved. Still, they all have in common that they are rich in serine and lysine, and have PTMs, although they may be somewhat different from the ones in *C. fusiformis* (De Tommasi et al., 2017).

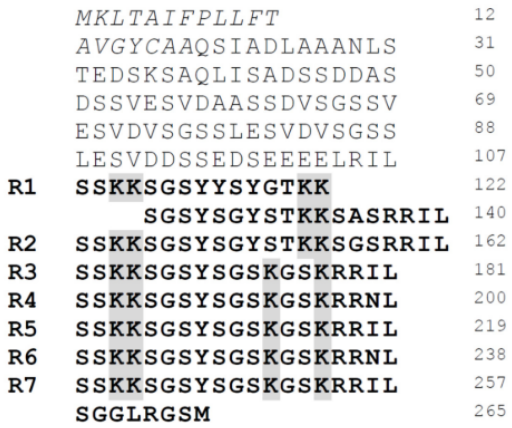

Figure 3.1: The amino acid sequence of the Silaffin-1 precursor protein (Sil-1p). The lysine residues are highlighted in grey, and the segments that result from proteolytic cleavage are noted R1-R7 (Kröger et al., 1999).

Sil-1A is known to precipitate nanospheres of silica *in vitro*. Since nascent frustules in the SDV are known to contain nanospheres, it is likely that the silaffins contribute to this formation *in vivo*. Comparing the nanospheres made from only Sil-1A and a combination of different silaffins it was seen that the nanospheres were remarkably different, with diameters of 500-700 nm and less than 50 nm, respectively. The ratio of positive and negative charges of the silaffins also affected the morphology of the precipitated silica. In addition, it has been suggested that the different amino acids in the middle of the KXXK motif can yield different size and morphology of the precipitated silica particles. All of these observations suggest that that silaffins take part in the nanoscale patterning of the frustule (Kröger et al., 1999).

Precipitation of silica is a naturally occurring process, although it is rather slow. Research has found that the presence of cations in a silica solution may help precipitate silica *in vitro* at a significantly higher rate. The cation flocculant attracts the silica during this process, and brings the individual silica particles together. Since silica biomineralisation in diatoms happens at a much faster rate than the regular precipitation rate, it is believed that a biological flocculant is present in the SDV. This could be the role of Sil-1A (Lechner and Becker, 2015). The proposed mechanism for the polycondensation reaction is not only based on the presence of cations, such as polyamines—they also depend on the negative charges, such as phosphate. The opposite charges of the molecules interact with one another, which has been seen to cause the self-assembly of the proteins. Further, this causes a phase separation and production of microdroplets. The interface between these droplets and the solution is the location of rapid polymerisation of silica, as

it contains a high density of polyamines and other cationic groups. At the surface, amino groups attract protons from the silicic acid, which yields a silanolate group. Silonate is a reactive molecule that attacks nearby silicic acid molecules in a condensation reaction. This reaction continues on new silicic acid molecules, until the resulting silica precipitates from the solution (Sumper, 2002).

The role of the polyamine PTMs has been confirmed using edited variants of the silaffins where the lysine residues are replaced by alanine. These proteins were non-functional, proving that the positive charge is key to be able to precipitate silica. In experiments, Sil-1A that lacked the phosphate PTM was not effective, but when phosphate was added to the solution, silaffin rapidly precipitated silica again. This confirmed that anions also are important for the mechanism (Kröger et al., 2002).

Sil-2, which only contains negative charges, is not able to precipitate silica on its own (Poulsen et al., 2003). Instead, it requires the presence of a cationic compound, e.g. by addition of long-chain polyamines (LCPAs). This should also be true for other silaffins that don't have cationic PTMs or have high presence of anionic PTMs (Lechner and Becker, 2015). The ratio between Sil-2 and Sil-1 or LCPA has shown to affect the size and morphology of the silica precipitate (Poulsen et al., 2003). Another feature of Sil-2 is that it inhibits silica formation when added to solutions of Sil-1 *in vitro*, which is contradictory to the effect it has shown to have on LCPA. In experiments with LCPA the precipitation rate reached a maximum, after which any further addition of Sil-2 showed an inhibitory effect on the LCPA's ability of silica precipitation. This is assumed to be because the anionic nature of Sil-2 at first helps the LCPA self-assemble, but later on will only shield the positive charges from the silicic acid, thereby inhibiting silica deposition (Poulsen et al., 2003). The same mechanism is thought to shield the polyamine PTMs that Sil-2 contains, as the abundance of anionic charges on the protein is thought to autoinhibit their function.

3.2 Cingulins

Cingulins are a family of proteins initially identified in the search of silaffin homologues in other species. A tool that compared the amino acid composition of the silaffins with the genome of *T. pseudonana* was used, as there does not seem to be a conservation of sequence in silaffins between species. The genome was screened for proteins containing sequences of more than 100 amino acids, of which more than 18 % were serine and more than 10 % were lysine. In addition, only proteins with a N-terminal signal peptide were considered. This screen yielded 89 genes. Of these, 6 were shown to be associated

with the cingulum of the cell walls, and were named cingulins accordingly. The cingulins have highly repetitive sequences. The CinY-proteins have alternating tyrosine (Y)-rich domains and KXXK-domains (similar to silaffins), and the CinW-proteins have alternating tryptophan (W)-rich domains, Y-/W-rich domains and KXXK-domains (Figure 3.2). In addition they have an RXL cleavage side on one end, and a signal peptide for co-translational transport into the ER (Scheffel et al., 2011).

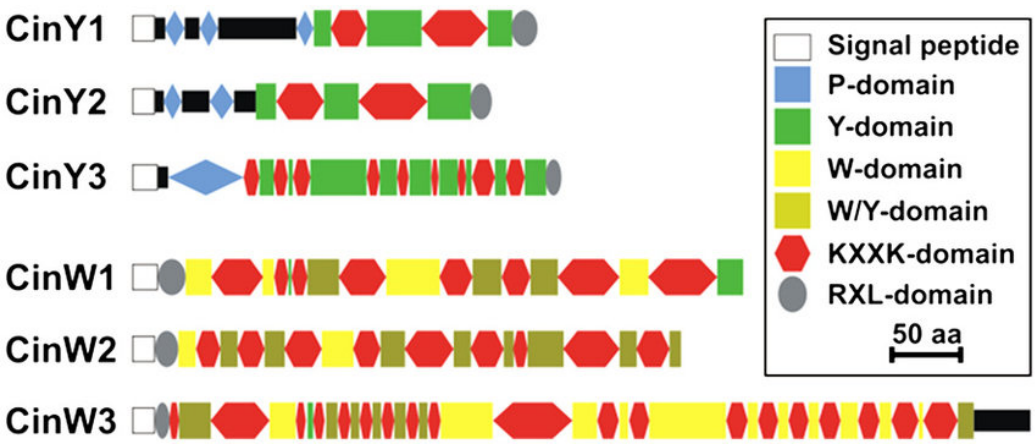

Figure 3.2: A representation of the 3 Y-cingulins and the 3 W-cingulins. The domains are depicted using different colours and shapes (Scheffel et al., 2011).

In studies of the cingulins in *T. pseudonana*, fluorescent fusion proteins located the cingulins exclusively in the girdle bands. When ammonium fluoride was added to the cells, the fluorescent cingulins did not solubilise, similarly to silaffins, making them a part of the AFIM of the microrings (Scheffel et al., 2011). Further research has shown that cingulins are also present in the microplates. In fact, microrings and microplates have been shown to have a highly similar amino acid composition to the cingulins, suggesting that they are the major components. One exception was that the microrings and microplates didn't have as high lysine content as the cingulins. This may be due to PTMs of the lysine residues, which make them less detectable (Kotzsch et al., 2016).

Cingulins have been shown to aggregate at acidic pH. Aqueous solutions containing CinY-proteins aggregate only at high salt concentrations, and CinW-proteins aggregate at low salt concentrations. They do, however, need some presence of salt to solubilise in aqueous solutions. If a mix of the two are in a solution together, they will aggregate either way (Kotzsch et al., 2016). The connection between the proteins is thought to be due to aromatic

and hydrophobic interactions of the tryptophan and tyrosine residues. In addition, some cingulins have acidic and some have basic pI, which should cause ionic interactions between the charges of the different proteins (Scheffel et al., 2011). The aggregation of cingulins is thought to be the first step of the assembly of AFIMs in the SDV. Further on, it is believed that the aggregates are stabilised by cross-linking, by e.g. O-phosphoester or O-glycosidic bonds, which is likely to account for the insolubility of the AFIM (Kotzsch et al., 2016).

Cingulins have been found to precipitate Si *in vitro*, which is assumed to be due to the high presence of cations on the protein, such as in the silaffins. What differs from the silaffins, however, is the fact that the cingulins are able to precipitate silica even without PTMs. At a closer look, the cingulins contain a higher amount of positively charged amino acids, mainly lysine, which is why they are able to precipitate silica on their own. Although there has not been much research on this subject yet, it is likely that PTMs would still make the precipitation accelerate. CinY-proteins precipitated silica at a faster rate than CinW-proteins in previous experiments, which might be due to the ratio of positive to negative charges. For example, CinY2 has a ratio of 2.2, while CinW2 has a ratio of 1.2. As CinW-proteins have more negative charges they may shield the positive charges, thereby slowing down the reaction. This is similar to what has also been seen in Sil-2 (Kotzsch et al., 2016).

3.3 Silacidins

The silacidins were discovered in experiments involving silaffins in *T. pseudonana*. When the silaffin Sil1/2L was subjected to size exclusion chromatography under high salt concentrations, a previously unknown protein with a low molecular weight was identified. The new peptide was unable to be sequenced unless first treated with HF, suggesting that it contained many PTMs in its native state. Sequencing identified three similar amino acid-sequences, denoted silacidin A, B and C, and a search in the *T. pseudonana* genome database recognised these as parts of the same open reading frame. The sequence is presented in Figure 3.3. Looking at the sequence there is a RRL protease cleavage site separating each of the sequences, similarly to the RXL motifs that have been seen in other frustule-associated proteins. This indicates that the proteins have analogous processing pathways. The suggested PTMs have been further investigated by Edman sequencing of the native protein. The sequencing yielded no serine compounds, which implies that the serine residues are the targets of the PTMs, and further investigation using NMR showed that the serines had been phosphorylated. In addition

to phosphoserines, the silacidins had a high content of aspartic and glutamic acid, making the peptide highly acidic (Wenzl et al., 2008).

Because of the polyaninionic nature of the silacidins they are believed to take the same role as dissolved phosphate or Sil-2 in silica precipitation; that is, they accelerate the precipitation rate significantly. The negative charges were seen to be key to causing self-assembly in e.g. silaffins. The same association should be valid for silacidins, which would explain why they were so tightly bound to Sil1/2L when they were first discovered (Wenzl et al., 2008). What is unique about silacidins compared to other known anionic molecules is that they are able to help precipitate silica at very low silicic acid concentrations. In fact, the silacidins are able to precipitate at concentrations that are only a third of that of pure phosphate. This attribute could be an important factor in ensuring silica precipitation in silicic acid depleted habitats. This role was confirmed by observing a increase in expression during silica starvation (Richthammer et al., 2011).

Figure 3.3: The amino acid of the silacidin precursor protein. The RRL cleavage site is denoted in red and the sites that differ for each of the segments are denoted in blue (Wenzl et al., 2008).

An experiment downregulating the transcription of the silacidin precursor protein resulted in a large valve of *T. pseudonana*. This indicates that one of the roles of silacidins is to restrict the size of the diatom cells. This could be useful in species that sexually reproduce, as the hypotheca grows smaller for each generation. *T. pseudonana* does not sexually reproduce, however, so this correlation could not be confirmed. Other situations where a smaller cell could be useful is under nutrient limitation. Even if the limited nutrient isn't necessarily silica, a smaller volume/surface ratio could benefit uptake into the cell. By decreasing the temperature of the cultures, the cell size also increased significantly, accompanied with a downregulation of silacidins.

Temperature change did not affect transcription of any other known frustule-producing proteins, strengthening the likelihood that silacidins take part in the process (Kirkham et al., 2017).

3.4 Silicalemma-associated proteins

Silicalemma-associated proteins (SAPs) are a recently discovered family of proteins that span the silicalemma. Together with silicanins, these are suspected to take part in the communication between cytoskeleton and the frustule through the silicalemma (Tesson et al., 2017). They were first discovered in a transcriptomics analysis of *T. pseudonana*, as it had a similar expression to Sil-3 (Shrestha et al., 2012), and has later on been found in several diatom species. The SAPs have a N-terminal signal peptide for co-translational transport into the ER and a single transmembrane domain. The C-terminal is suggested to interact with the cytoskeleton, and is conserved between species. Each SAP also contains several RXL protease cleavage sites, as has been seen in several other silica-associated proteins. They do not contain the KXXK-domain that has been seen in known silica-polymerising proteins; however, they are suggested to contain several phosphorylated serine residues, which could have the same roles as the negatively charged silaffins in silica-polymerisation (Tesson et al., 2017).

T. pseudonana knock-down mutants of SAP1 and SAP3 were observed to have an altered valve morphology, providing two distinct phenotypes. The difference suggests that these two proteins have different roles in frustule formation. The SAP1 knock-down had a clearly misplaced pattern centre, and a unstructured mesoscale pattern on the distal valve suface. Because the knock-out yielded two different effects on the valve, it was suggested that the SAP1 protein was involved in two separate process in frustule formation; positioning of the pattern centre through placement of the primary site of silification and distal surface silica deposition. The SAP3 knock-out affected the z-axis expansion of the ribs and cross-links, leaving the base layer of the valve exposed. Thus, it was suspected that SAP3 is involved in aggregation of silaffins and LCPAs along the base layer ribs, thereby yielding silica precipitation (Tesson et al., 2017).

3.5 Long-chain polyamines

Long-chain polyamines, or LCPAs, are molecules that are assumed to have similar effects as the silaffins when it comes to silica polymerisation. They were discovered when looking for organic constituents of the frustule, by hydrogen fluoride-extracts of the silica (Kröger et al., 2000). The LCPAs

are major constituents of most diatom frustules, and in most species they are found in equal quantity to the silaffins. The LCPAs show a structure that is highly similar to the post-translationally attached side-chains of silaffins. They usually have a spermidine, putrescine or propylenediamine basis molecule attached to n oligo-propyleneimine units. It is common that some or most of the nitrogen molecules have been N-methylated, internally or externally (Sumper and Brunner, 2006). The structure of the three LCPAs found in *T. pseudonana* are illustrated in Figure 3.4.

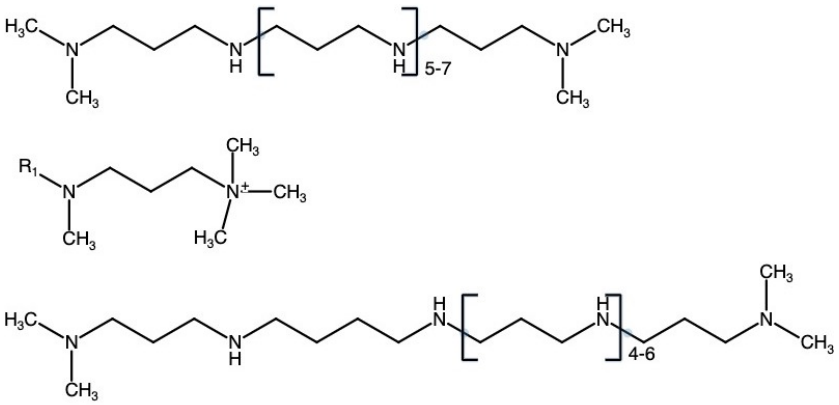

Figure 3.4: The structure of the LCPAs found in *T. pseudonana* by Sumper and Brunner (2006).

By isolating the LCPAs and adding them to siliceous solutions they were shown to precipitate silica *in vitro*. Different LCPAs yielded different sizes and morphologies of the precipitated particles, and mixtures of the different types were shown to give a combination of the individual morphologies. The silica that was deposited showed resemblance to silica found *in vivo*, which is why it was hypothesised that they took part in the process of frustule formation of diatoms. The results from these experiments are similar to what has been found in silaffins, which conforms with their strikingly similar structure. The two groups are therefore thought to act equally when it comes to silica polymerisation (Kröger et al., 2000). The size of the silica particles have been studied through dynamic light scattering. Silica formation has been studied by Sumper (2004), where silica solutions with or without addition of LCPAs was examined over time. Here, the results showed that pure silica solutions had a linear growth over time. In comparison, solutions with LCPA had a significantly faster growth rate in the beginning, but ceased to grow at a low diameter within only a few minutes.

3.6 Chitin

Chitin is a carbohydrate that is built up of N-acetylclucoseamine monomers (Figure 3.5) by chitin synthases. In diatoms the chitin fibers lie parallell to each other, creating a highly crystalline structure. Chitin is produced by chitin synthases, of which there are several kinds. These synthases have three motifs in common, which is QXXEY, EDR and QXRRW, which are responsible for reaction catalysis and substrate specificity. Because of this similarity it is assumed that the proteins have a common ancestral origin, but that they have diversified at a later point in time. The different synthases are responsible for synthesising chitin at different locations in the cell, and for different purposes. The chitin synthases have been divided into three phylogenetic groups or clades; A, B and C. Clade A is not assumed to take part in the cell wall, but both clade B and clade C are. The transcription of the two latter are upregulated when stress is inflicted on the cells, such as during nutrient depletion. In addition, expression of clade B proteins shift during regular cell cycle progression (Durkin et al., 2009).

Chitin is present at several locations in the diatoms. It has long been known that chitin fibers protrude from the rimo- and fultoportulae of species such as those belonging to the *Thalassiosirales* order, which has been thought to contribute to controlling the buoyancy of the cells in open waters (Hildebrand et al., 2006). Chitin was also observed in the girdle bands during starvation, which is in accordance with the elongation that commonly develops in starving diatom cells (Durkin et al., 2009). An experiment by Li et al. (2016) investigated how chitinase-producing bacteria affected the diatom *T. pseudonana*. The bacteria proved algicidal, and it was revealed that chitinase was the cause. It became evident that that the chitin is an essential

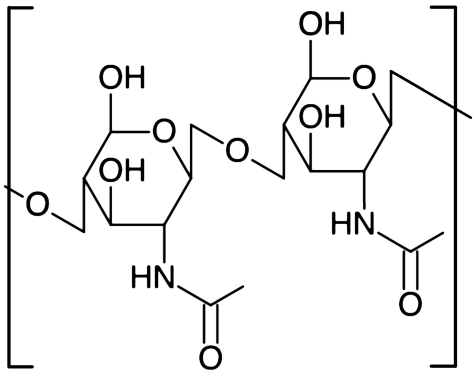

Figure 3.5: The chemical structure of chitin. The carbohydrate is built up of n repeating units as shown. Adapted from Ehrlich (2010).

structural element in the diatom cell wall. In *T. pseudonana*, a significant amount of chitin is integrated in the silica of the frustule. This chitin is more disordered than the highly crystalline structure of the external chitin fibers. By extracting the chitin from the silica using NH_4F it was observed that the size and shape of the chitin network within the frustule was similar to that of the silica, which indicated a role in the patterning of the frustule (Brunner et al., 2009).

3.7 Non-biomineralising proteins involved with the frustule

Frustulins were the first frustule-associated proteins to be identified. They were initially extracted from the membrane of the *C. fusiformis* using EDTA (Kröger et al., 1994). 5 different frustulins have been identified, which are separated by the size of the fragments. They have been found in both pennate and centric diatoms, and can be identified by a presence of three or more of the following domains: presequence domain, ACR domain, Proline-rich domain, poly-glycine domain and tryptophan-rich domain. The presequence domain is assumed to take part of intracellular transport of the frutulins into the SDV, while the Proline and poly-Glycine domains are expected to be used as stiff spacer arms for separating the different parts of the frustulins. The ACR domain is highly conserved between species, and is therefore believed to be an essential part of frustulins (Kröger et al., 1996). The domain has been observed to bind to Ca^{2+},which has lead to the belief that it uses Ca-bridges to bind to the frustule, organic casing or other proteins (Kröger et al., 1994; Kröger et al., 1996). The frustulins are not thought to take part in the silica biomineralization process itself, as it is not associated with the frustule until after silica deposition is completed (van de Poll et al., 1999). It is rather believed that the the frustulins may serve as protection of the silica against corrosion, as it lays in a layer around the exocytosed frustule (Bidle and Azam, 1999; van de Poll et al., 1999).

The pleuralins are proteins that have been associated with the pleural bands in some species. They are located on the proximal side of the pleural bands of the epitheca, where they cover the surface of the silica (Kröger and Wetherbee, 2000). The pleuralins are tightly bound to the frustule and can only be released from the silica using hydrogen fluoride treatment. Thus, it is assumed that the pleuralins are bound to either the silica itself or other proteins on the frustule (Kröger et al., 1997). The defining characteristic of the pleuralins is the PSCD domains, which are rich in proline, serine, cysteine and aspartate, and a N-terminal signal peptide for co-translational transport into

the ER. They have not been seen to precipitate silica in vitro, so the proteins are not expected to be involved in silica formation. The PSCD domains have, however, been seen to bind non-covalantly to Sil-1 *in vitro*, which could be the reason for the strong connection between the pleuralins and the frustule. They have also been observed bound to frustulins through Ca-bridges *in vitro*, and so it is likely that they bind to both silaffins and frustulins *in vivo* (Figure 3.6). This could further aid in connecting the interface between the epitheca and the hypotheca (De Sanctis et al., 2016).

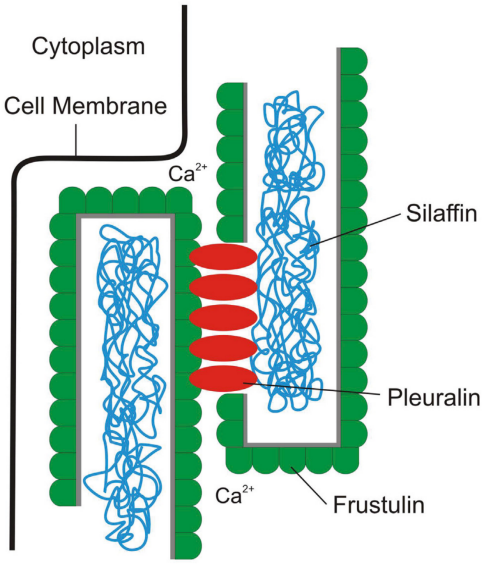

Figure 3.6: A model of how the pleuralins could be connected to the frustulins and silaffins *in vivo* (De Sanctis et al., 2016).

p150 is a protein that has been seen upregulated in copper-stressed *T. pseudonana*. Although the sequences are not homologous, p150 has highly similar biochemical similarities to pleuralins. Pleuralins have not been detected in centric diatom species, unlike p150, and so the two types of protein may have similar functions in different species. p150 also has a chitin-binding domain and a RGD motif that is known for cell adhesion, both of which could be used for attachment similar to what is suggested for the pleuralins (Davis et al., 2005). Expression is upregulated during several stressful situations, which often are accompanied with elongation of the cells. As p150 and other p150-like proteins are seen in connection with the girdle bands, it it not unlikely that they may be involved in stabilising the cells during the process of elongation (Durkin et al., 2009; Davis et al., 2005).

4 Results

4.1 Identification of the most fluorescent clones

After conjugation, two new generations of transformants were picked. The most fluorescent clones were decided by flow cytometry in order to decide which clones to use for further experimentation. See Figure 4.1 for the second generation of transformants. Here, the Tp24711-2.4 and Tp24711-2.9 transformants were chosen for further use, as they expressed the most fluorescence. For the third generation, seen in Figure 4.2, the Tp24711-3.12 transformant expressed the highest mean fluorescence. However, it had a very low fraction of alive cells (0.8 %), and so the Tp24711-3.11 transformant was used in stead.

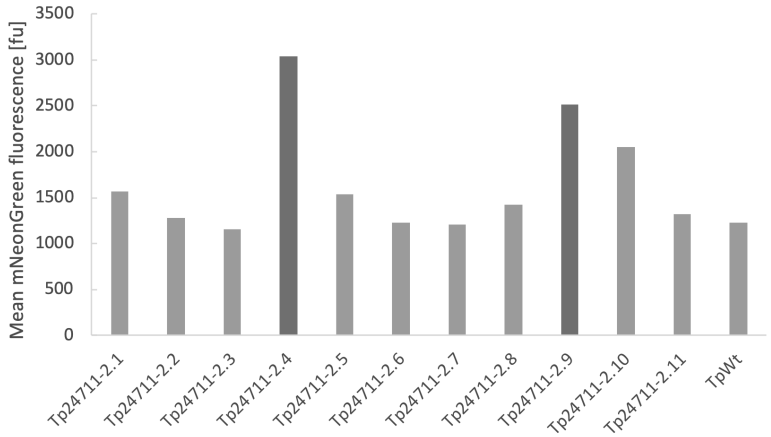

Figure 4.1: The mean fluorescence (in the range 533 ± 30 nm) expressed by the different mNeonGreen-Tp24711 transformant clones of the second generation. Wild-type *T. pseudonana* was also analysed and is plotted for comparison. The Tp24711-2.4 and Tp24711-2.9 transformants are marked in a darker shade as they expressed the most fluorescence and were chosen to be used for further studies.

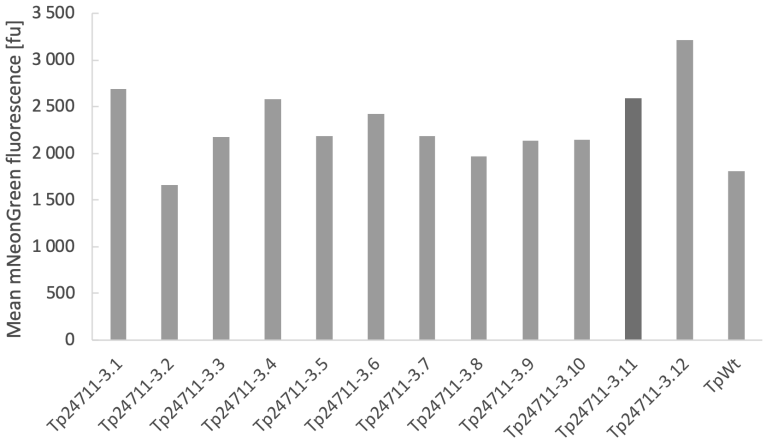

Figure 4.2: The mean fluorescence (in the range 533 ± 30 nm) expressed by the different mNeonGreen-Tp24711 transformant clones. Wild-type *T. pseudonana* was also analysed and is plotted for comparison. The Tp24711-3.11 transformant is marked in a darker shade as it was chosen to be used for further studies.

4.2 Synchronisation experiments

Three synchronisation experiments were done in total. These were going to help confirm what has previously been found on the expression pattern of Tp24711 by Gresseth (2019).

4.2.1 The first synchronisation experiment

In the first synchronisation experiment the cultures were starved for 24 hours. Progression of cell density and fluorescence during the first synchronisation experiment is shown in Figure 4.3. The cell density of both transformants and the wild-type were stable during most of the 5 hours of the experiment (Figure 4.3a). The wild-type culture had a small increase in density from 4 to 5 hours, and the Tp24711-1.5 had a decrease. There were peaks in fluorescence of 100 000–400 000 fu at 0 and 2 hours after Si-addition (Figure 4.3b). Because these peaks were also seen in the wild-type culture, it was deemed probable that there was something wrong with the measurements.

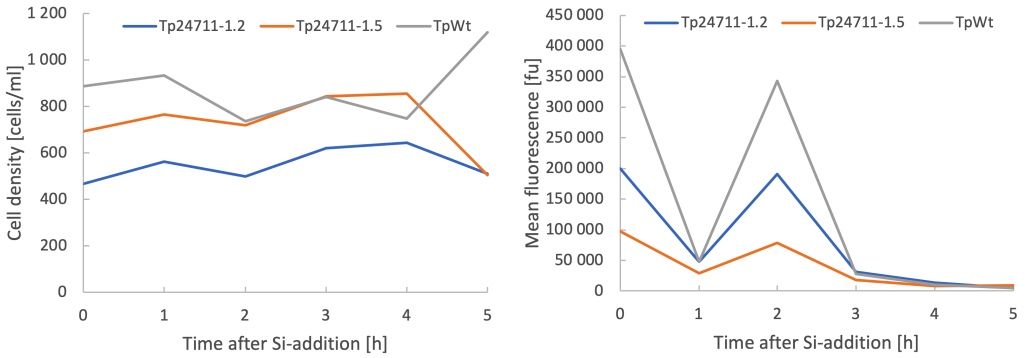

(a) Cell density (b) Mean mNeonGreen fluorescence

Figure 4.3: The (a) cell density and (b) mean mNeonGreen fluorescence plotted as a function of time after addition of silica in the first synchronisation experiment. The three cultures measured were the two transformant cultures from Tp24711-1 and a wild-type culture for reference.

4.2.2 The second synchronisation experiment

In the second synchronisation experiment the cultures were starved for 24 hours, and the cell density was adjusted prior to starvation. The cell density and fluorescence measurements of the second experiment are shown in Figure 4.4. These show a modest, continuous cell growth for Tp24711-1.2 and TpWt, while Tp24711-1.5 had several small peaks (Figure 4.4a). The

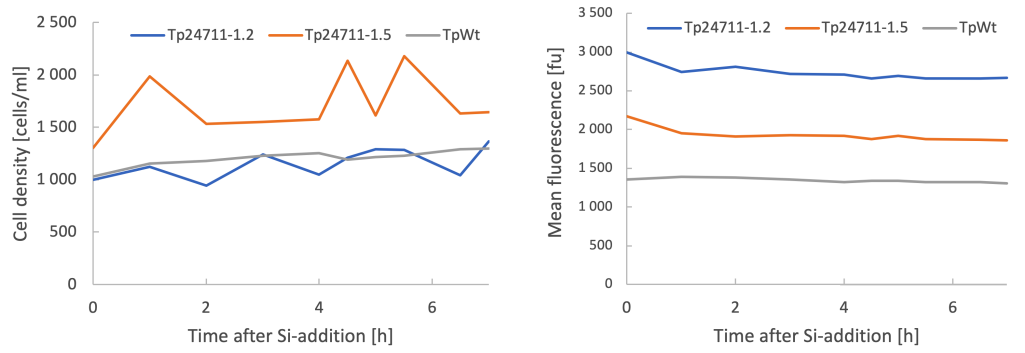

(a) Cell density (b) Mean mNeonGreen fluorescence

Figure 4.4: The (a) cell density and (b) mean mNeonGreen fluorescence plotted as a function of time after addition of silica in the second synchronisation experiment. The three cultures measured were the two transformant cultures from Tp24711-1 and a wild-type culture for reference.

latter fluctuated between 1 500 and 2 000 cells/µl. The fluorescence was stable for all the samples during the entire experiment, where TpWt emitted the least fluorescence (Figure 4.4b). The results were discarded due to the fluctuating cell density.

4.2.3 The third synchronisation experiment

In the third synchronisation experiment the cultures were starved for 48 hours, and the cell density was adjusted prior to starvation. The third synchronisation experiment yielded the results shown in Figure 4.5. The datapoint at 1h for the Tp24711-1.5 culture was discarded as faulty data, and is illustrated by a dotted line. Both transformant cultures had an even cell density in the beginning, with a sudden increase between 8 and 9 hours for Tp24711-1.2, and between 3 and 4 hours for Tp24711-1.5 (Figure 4.5a). The Tp24711-1.2 culture also had a small increase in cell density for the first hour after Si-addition. TpWt did not show any significant growth in cell density during the experiment. The mean mNeonGreen fluorescence decreased approximately 20 % for both of the transformants during the experiment (Figure 4.5b). TpWt emitted a stable fluorescence, which was consistently lower than both transformants.

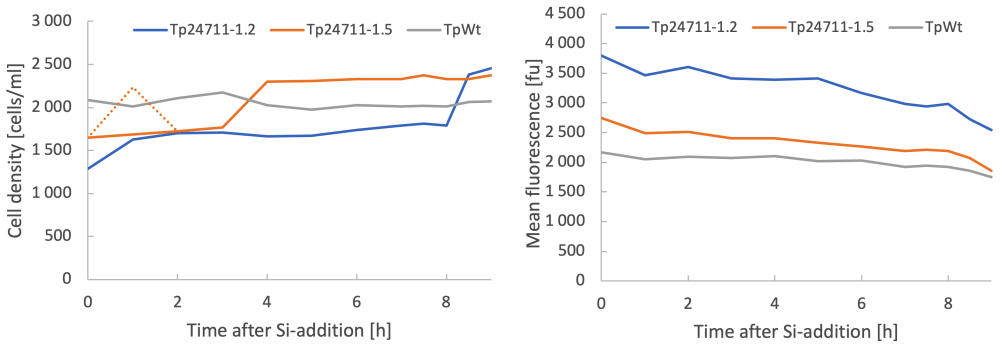

(a) Cell density (b) Mean mNeonGreen fluorescence

Figure 4.5: The (a) cell density and (b) mean mNeonGreen fluorescence plotted as a function of time after addition of silica in the third synchronisation experiment. The three cultures measured were the two transformant cultures from Tp24711-1 and a wild-type culture for reference. The dotted line represents a data point that was discarded, as it deviated significantly.

4.2.4 Cell stage determination

A cell stage determination was done in order to compare the observed results in Figure 4.5 with the cell cycle. The cell cycle can be estimated from seeing when the cells divide, but a cell cycle determination yields more accurate results. The results are given in Figure 4.6. In the Tp24711-1.2 culture 81 % of the cells were in S at the first measurement, but it decreased to 20-30 % for the last 5 hours. Meanwhile, only 4 % of the cells were in G1 in the beginning, but it increased to approximately 50 % for the last hours of the experiment. There were 13 % cells in G2+M in the beginning, but it decreased rapidly. Then, another boost in G2+M was seen, with a peak at 5 hours. For the Tp24711-1.5 culture the cells were approximately 50-60 % in G1 and 30-40 % in the S phase during the entire experiment. The cells

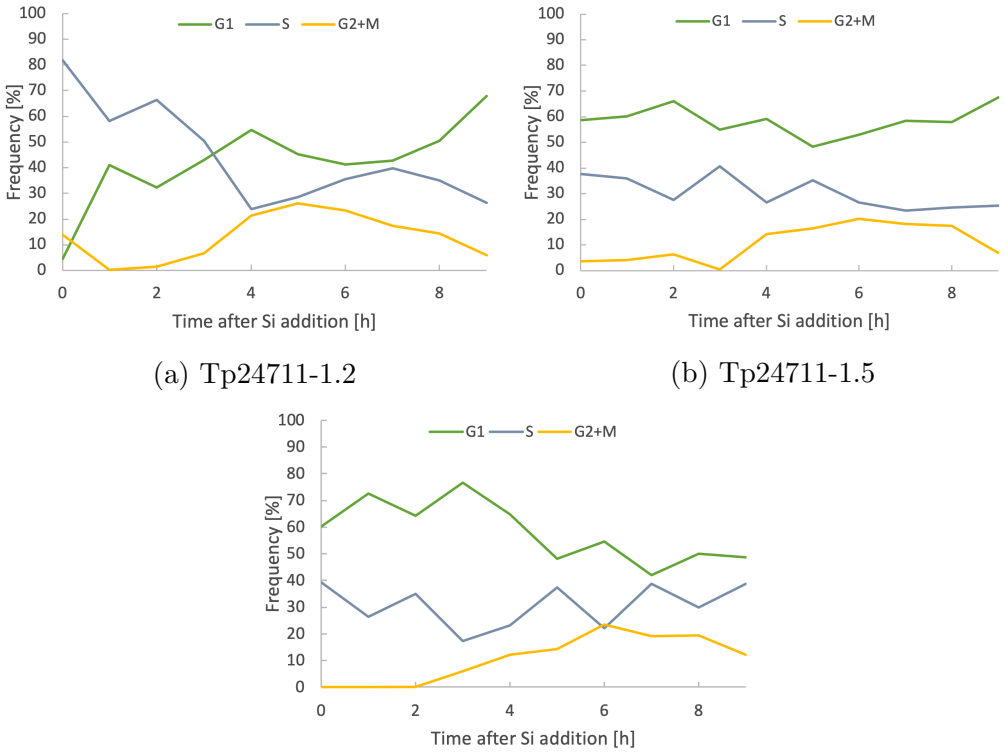

(a) Tp24711-1.2

(b) Tp24711-1.5

(c) TpWt

Figure 4.6: Cell stage determination of the (a) Tp24711-1.2 and (b) Tp24711-1.5 transformants and (c) the wild-type control during the third synchronisation experiment. The percentage of cells in each cell stage is plotted as a function of time after Si-addition.

were in G2+M both in the first two hours (6 %), and then again for the last 5 hours (15-20 %). After the experiment ended at 9 hours there were approximately 7 % cells in G2+M.

For the TpWt culture most cells (50-80 %) were always in G1, while most of the rest were in S (20-40 %). They showed no clear pattern for growth. There were no cells in G2+M for the first 2 hours of the experiment. Then, the G2+M phase increased to a peak at 6 hours of 20 %, with a small decline to 10 % after 9 hours.

The output plot from Tp24711-5 at 7 hours is given as an example in Figure 4.7. The cell cycle analysis in 4.7a shows that the G1 and S phase overlapped considerably, while the G2+M phase was more separated from them. The majority of the cells were predicted by the NovoExpress® software to be in G1, while approximately equal amounts of cells were in S and G2+M. The scatter plot in 4.7b shows the size of the cells (Fsc) plotted as a function of SYBR green fluorescence. The events used in 4.7a were taken from the P2 gate in 4.7b. The cell cycle analysis plot was very selective about how the gate was placed in order to yield results, which resulted in different size and shapes for the gates in every sample.

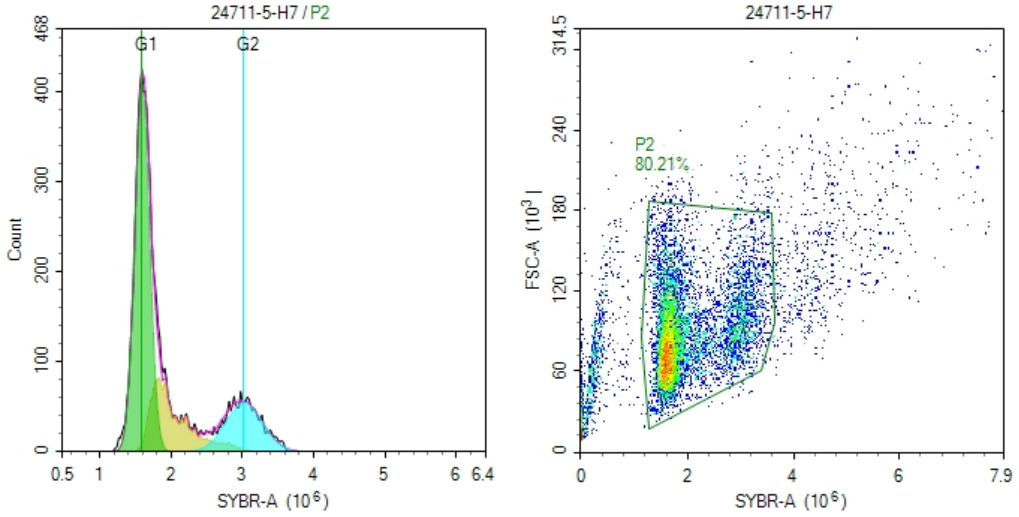

(a) Cell cycle determination

(b) Gating for desired cells

Figure 4.7: Output from the Tp24711-5 cell cycle analysis of the third synchronisation experiment 7 hours after Si-addition. (a) The cell cycle analysis shows the predicted fraction of cells for G1, S and G2+M are given in green, yellow and blue, respectively. (b) The Fsc plotted as a function of fluorescence intensity in the range of SYBR green. The events inside the gate in (b) were used in plotting (a).

4.3 Microscopy of mNeonGreen-Tp24711 transformants

The three generations of mNeonGreen-Tp24711 transformants were studied in either confocal or fluorescence microscopes. The first generation of transformants originated from the previous experiment of Gresseth (2019), while the second and third generation originate from the same new transformation, but were picked at different occasions. All the cells were imaged for fluorescence in the green and red spectre, in addition to brightfield. The red fluorescence images illustrate autofluorescence that was emitted from the chloroplasts. The green fluorescence images illustrate the fluorescence emitted from mNeonGreen, in addition to autofluorescence.

4.3.1 Tp24711-1

The Tp24711-1 transformants were observed in both a fluorescence microscope and a confocal microscope (results not shown). The cells were not observed to express any fluorescence outside of the autofluorescence. The cells looked similar to what will be shown in Sections 4.3.2 and 4.3.3.

After 2 months in storage in the dark at 12 °C, new images were taken from the Tp24711-1 cultures. The new images differed what had been observed months before, as they emitted fluorescence in the green spectre outside of the autofluorescence. This is seen in Figure 4.8. The mNeonGreen fluorescence circumferences the cingulum of two of cells, and is clearly separated from the red autofluorescence.

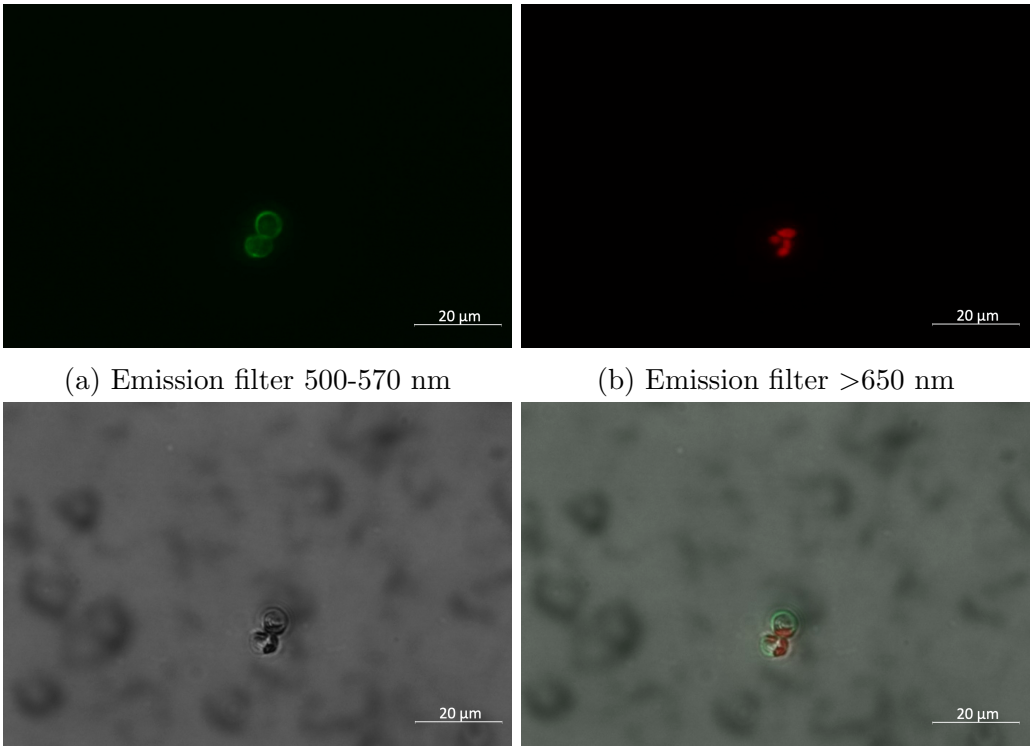

(a) Emission filter 500-570 nm

(b) Emission filter >650 nm

(c) Brightfield

(d) Overlaying images

Figure 4.8: Fluorescence microscopy imaging of the Tp24711-1 transformants after they began expressing mNeonGreen fluorescence anew. Fluorescence emitted from the cells in the range of (a) mNeonGreen (505-555 nm) and (b) autofluorescence (>650 nm), while (c) shows brightfield imaging. All three images have been overlayed in (d).

Another image was taken of the fluorescent Tp24711-1 transformants in a confocal microscope (Figure 4.9). On the right side there are two adjoining cells that seem to have been parted recently. These show fluorescence in their newly formed valves, in addition to a faint fluorescence surrounding the entire surface of the cell. Other cells concurred with this, and also emitted fluorescence in the green spectre outside of autofluorescence.

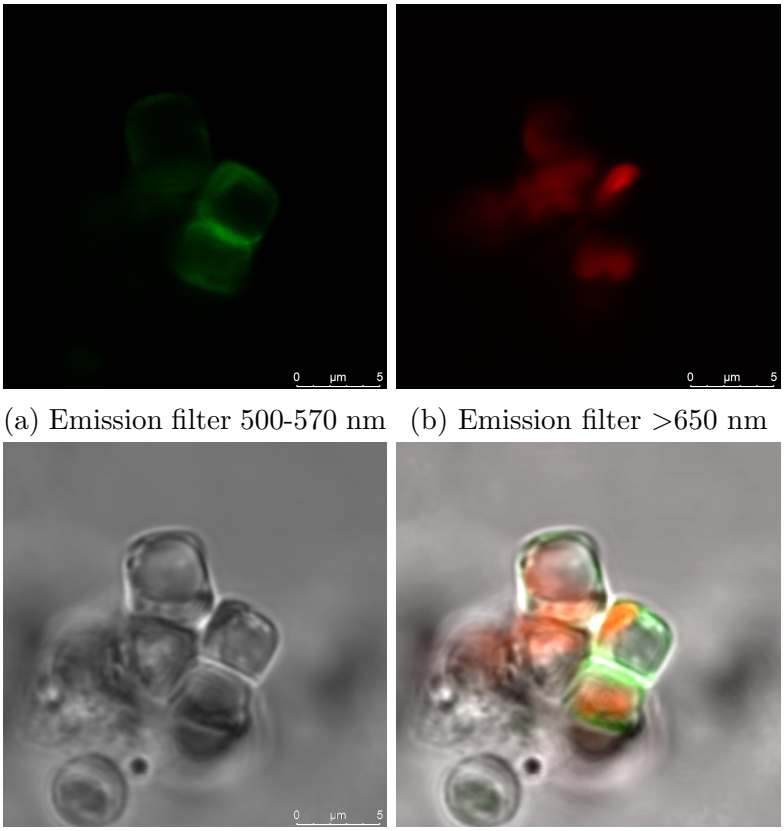

(a) Emission filter 500-570 nm (b) Emission filter >650 nm

(c) Brightfield (d) Overlaying images

Figure 4.9: Confocal microscopy imaging of the Tp24711-1 transformants when they expressed mNeonGreen fluorescence. Fluorescence emitted from the cells in the range of (a) mNeonGreen (500-570 nm) and (b) autofluorescence (>650 nm), while (c) shows brightfield imaging. All three images have been overlayed in (d).

4.3.2 Tp24711-2

Images of the Tp24711-2 transformants is shown in Figure 4.10. Here, the red and green fluorescence have been imaged from the same cells, in addition to a brightfield image. There was only a little fluorescence emitted in the green spectre, and this overlaps well with the autofluorescence, which is illustrated through the red fluorescence. It is therefore reasonable to assume that no mNeonGreen fluorescence was emitted from these cells. Several other cells were investigated using both confocal and conventional fluorescence microscopy, all of which illustrated the same as Figure 4.10.

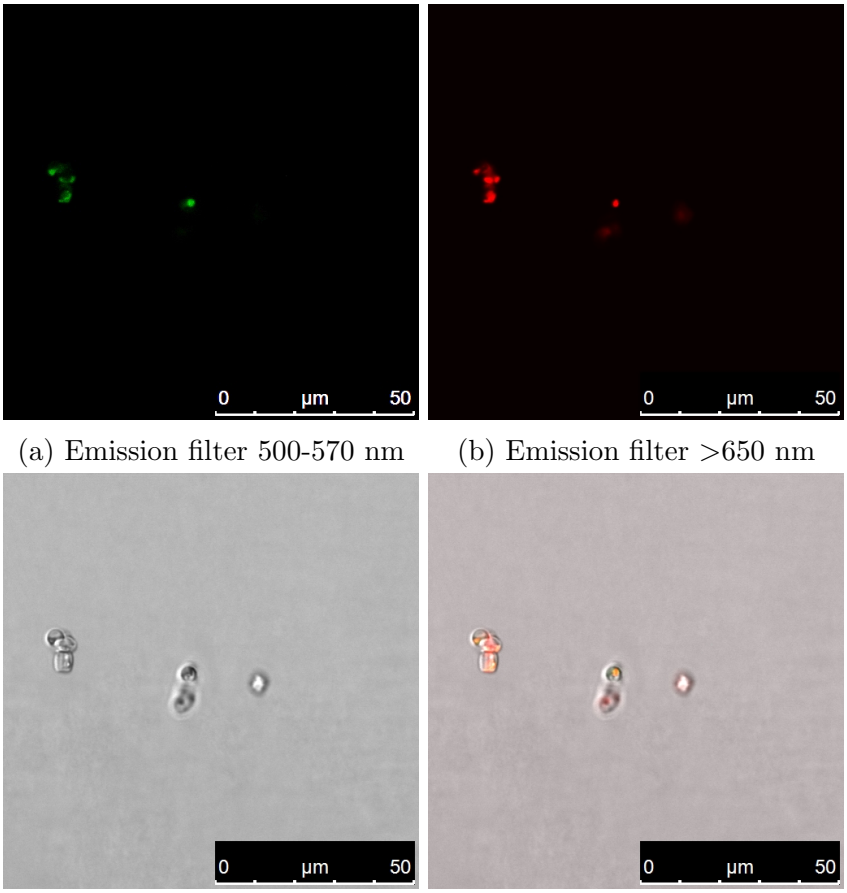

(a) Emission filter 500-570 nm (b) Emission filter >650 nm

(c) Brightfield (d) Overlaying images

Figure 4.10: Confocal microscopy imaging of the Tp24711-2.9 transformants. Fluorescence emitted from the cells in the range of (a) mNeonGreen (500-570 nm) and (b) autofluorescence (>650 nm), while (c) shows brightfield imaging. All three images have been overlayed in (d).

4.3.3 Tp24711-3

Figure 4.11 shows two cells, with fluorescence emitted in both ends of each cell. Looking at Figure 4.11a and 4.11b it is likely that the fluorescence was caused by the autofluorescence of the two chloroplasts of the cells. These overlapped completely with the green fluorescence seen in 4.11a, which makes it likely that the two cells do not emit any mNeonGreen fluorescence. The same was observed for all the investigated cells.

The results from the different generations show that all of the transformants failed to express mNeonGreen fluorescence at some point.

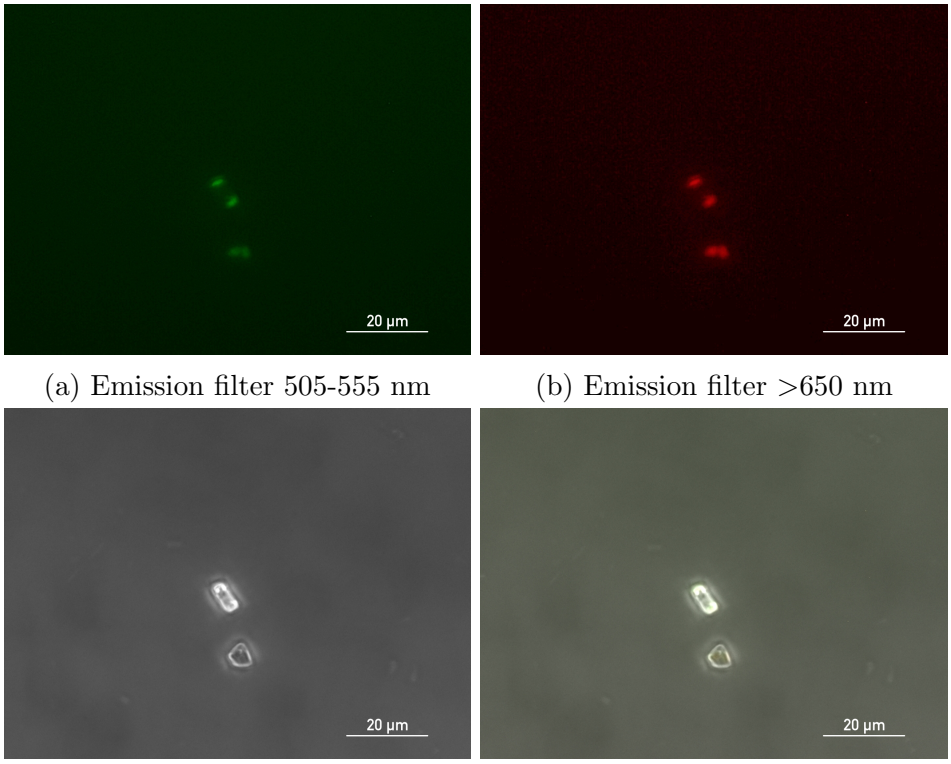

(a) Emission filter 505-555 nm (b) Emission filter >650 nm

(c) Brightfield (d) Overlaying images

Figure 4.11: Fluorescence microscopy imaging of the Tp24711-3.11 transformants. Fluorescence emitted in the range of (a) 505-555 nm and (b) >650 nm is illustrated, while (c) shows brightfield imaging. All three images have been overlayed in (d).

4.4 Flow cytometry of fluorescent Tp24711-1 transformants

After the Tp24711-1 transformants began to express mNeonGreen fluorescence again, the cultures were analysed on a flow cytometer in order to compare the mean mNeonGreen fluorescence with previous observations. The mNeonGreen fluorescence of the samples is given in Table 4.1. The fluorescence was considerably higher for both of the transformants compared to the wild-type.

Table 4.1: Mean mNeonGreen fluorescence emitted from the Tp24711-1 transformants after they regained their mNeonGreen fluorescence. A wild-type culture was also measured for comparison.

Culture	Mean mNeonGreen fluorescence [fu]
TpWt	1 653
Tp24711-1.2	11 659
Tp24711-1.5	8 748

4.5 Western blot

A western blot was done in order to identify whether the transformants expressed the mNeonGreen-Tp24711 protein. The blot of the Tp24711-1 transformants and TpWt is shown in Figure 4.12. Only the sample of the pelleted positive control showed on the western blot, which manifested in two bands of approximately 18 kDa and 25 kDa. The mNeonGreen protein of the positive control should be at 26.7 kDa, while the mNeonGreen-Tp24711 should have manifested at 75.7 kDa.

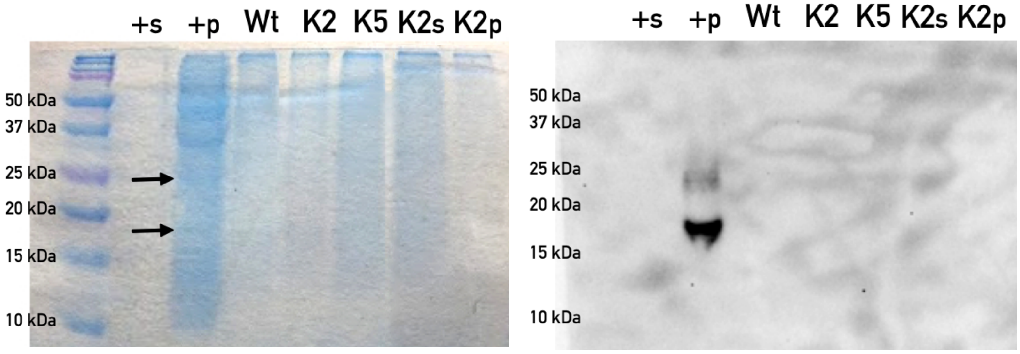

(a) Total protein content

(b) mNeonGreen antibody

Figure 4.12: Western blot of the Tp24711-1 transformants. (a) shows the total protein content of the different samples, while (b) shows the proteins that have associated with the antibodies for mNeonGreen. The black arrows in (a) indicate the location of the bands seen in (b). +; positive control, s; proteins derived from supernatant, p; proteins derived from pellet, Wt; wild-type, K2; Tp24711-1.2, K5; Tp24711-1.5.

4.6 Analysis of non-fluorescent transformants

A PCR was done in order to identify if a larger deletion or insertion had occurred to render the fusion gene ineffective. A gel electrophoresis of the non-fluorescent Tp24711-2 transformants yielded in the gel seen in Figures 4.13 and 4.14. The same bands were seen in both the Tp24711-2.4 and Tp24711-2.9 transformants, and so they are presented as one unit.

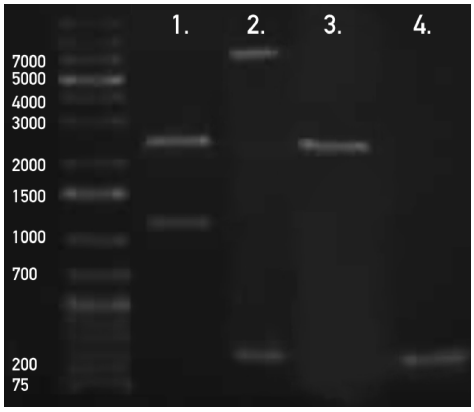

Figure 4.13: Gel electrophoresis of the PCR sample of the Tp24711-2 transformants with the 1. His3SeqF and mNeon-seqR and 2. His3SeqF and M13Rev primers. TpWt control with the 3. His3SeqF and mNeon-seqR and 4. His3SeqF and M13Rev primers.

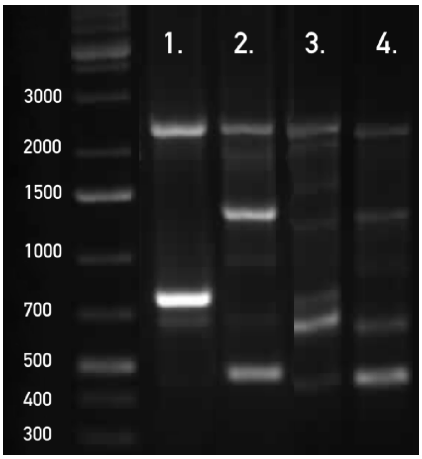

Figure 4.14: Gel electrophoresis of the PCR sample of the Tp24711-2 transformants with the 1. Tp24711-F1 and Tp24711-R1 and 2. Tp24711-F1 and Tp24711-R2 primers. TpWt control with the 3. Tp24711-F1 and Tp24711-R1 and 4. Tp24711-F1 and Tp24711-R2 primers

The sizes of the bands are summarised in Table 4.2. Several bands were seen for all the transformants, which is why the TpWt is presented next to it for comparison. By comparing the transformants and the wild-type, it was possible to deduce which bands were caused by the plasmid: 1 200 bp for the His3seqF/mNeon-seqR plasmid and 7 000 bp for the His3seqF/M13Rev. For the Tp24711-F1/R1 fragment it was harder to deduce, as all bands were the same fragment size, but differed in intensity. By excluding from intensity, the fragment should be approximately 800 bp. The Tp24711-F1/R2 fragment had the exact same sizes for both the transformants and the wild-type. None of the fragments matched with the expected fragment size.

Table 4.2: The expected size of the amplified fragments and the size of the bands that were run on gel. Most of the samples appeared as several bands per well. *represent two bands that were only barely visible, and blended over in the neighbouring bands.

Fragment primers	Clone	Expected size [bp]	Observed size [bp]		
His3seqF/mNeon-seqR	Tp24711-2	967	2 500	**1 200**	
	TpWt	-	2 500		
His3seqF/M13Rev	Tp24711-2	2 772	**7 000**	200	
	TpWt	-		200	
Tp24711-F1/R1	Tp24711-2	1 462	2 300	**800***	700
	TpWt	-	2 300	800	700*
Tp24711-F1/R2	Tp24711-2	1 987	2 300	1 400	500
	TpWt	-	2 300	1 400	500

4.7 The effect of cytoskeleton inhibitors

4.7.1 Titration of cytoskeleton inhibitors

After titration of inhibitors it was decided that following concentrations were going to be used for the inhibitor experiment:

Cytochalasin D	6 µM
Colchicine	40 µM
Oryzalin	0.2 µM

This decision was based on the results given in Appendix D.

4.7.2 The effect of cytoskeleton inhibitors on valve morphology

The cytoskeleton inhibitor-treated frustules were imaged using SEM in order to determine the inhibitors' effect on valve morphology. The wild-type control is given in Figure 4.15. The valve surface is similar as what has been imaged by N. Kröger (Figure 1.1), but has a more irregular shape of the fultoportula and rimoportulae. In addition, the cingulum of the cell was broken. This is coherent with what was observed for the other control valves.

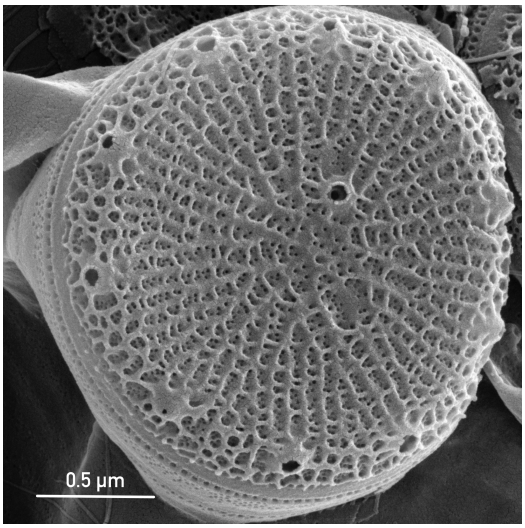

Figure 4.15: SEM of the valve of the control *T. pseudonana* frustule.

Two colchicine-treated valves are presented in Figure 4.16. In Figure 4.16a the valve ribs and cross-links are disorganised and in no particular pattern, which was characteristic for several of the studied frustules. In several of the frustules there were present 2 or 3 central fultoportulae, and some also had no fultoportulae. All control frustules contained only 1 fultoportulae. Several of the frustules also lacked large parts of their ribs and cross-links, as seen in Figure 4.16b, leaving only small remnants of the mesoscale structures.

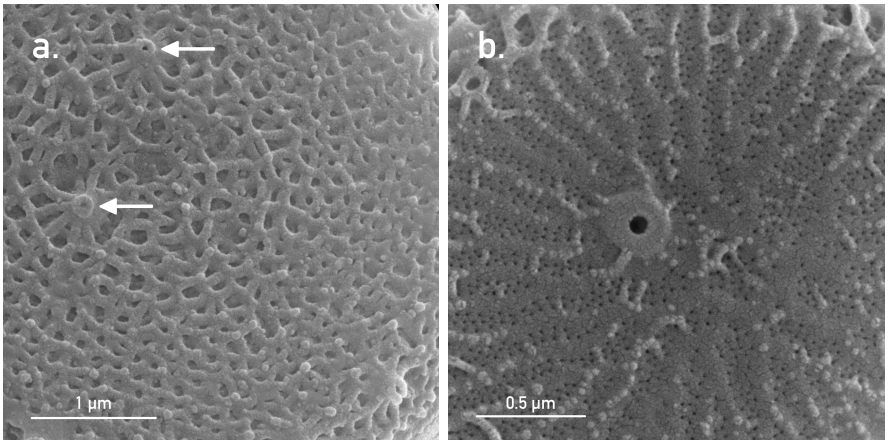

Figure 4.16: SEM of the effects of the microtubule inhibitor colchicine on valve structure. (a) The ribs and cross-links are largely overgrown, and there are two fultoportulae on the valve (arrows). (b) The ribs and cross-links are almost not visible, and only some small particles are left protruding from the valve surface.

A common feature of the oryzalin-treated frustules was overgrown ribs and cross-links as seen in Figure 4.17a, such as was observed in the colchicine-treated cells. This was often seen in combination with nanopores that were not visible (Figure 4.17b). Several of the oryzalin-treated frustules did not have a fultoportula, as seen in 4.17b.

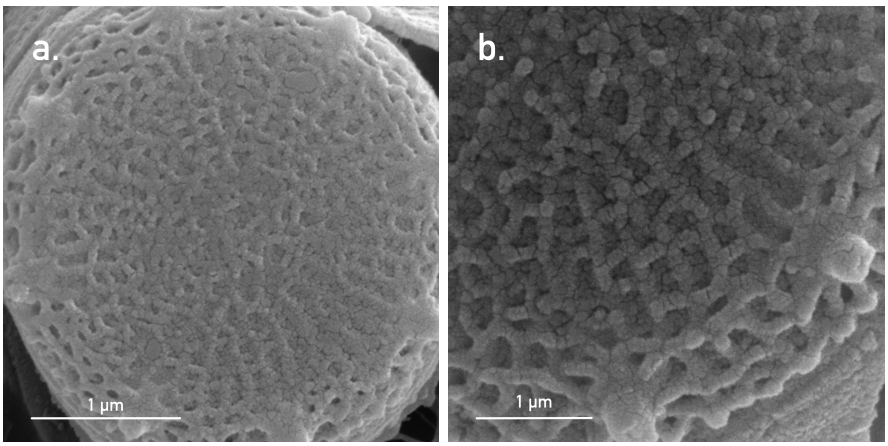

Figure 4.17: SEM of the effects of the microtubule inhibitor oryzalin on valve structure. (a) The valve is largely overgrown by ribs and cross-links, and there is no central fultoportula. (b) The valve surface shows overgrown ribs and cross-links, in addition to the nanopores not being visible.

In the cytochalasin D-treated valves the ribs and cross-links were mostly missing, as seen in Figure 4.18a. The pattern of the ribs were visible in the valve, put they didn't protrude from the valve surface as is seen in the control. Several of the investigated frustules also lacked a central fultoportulae.

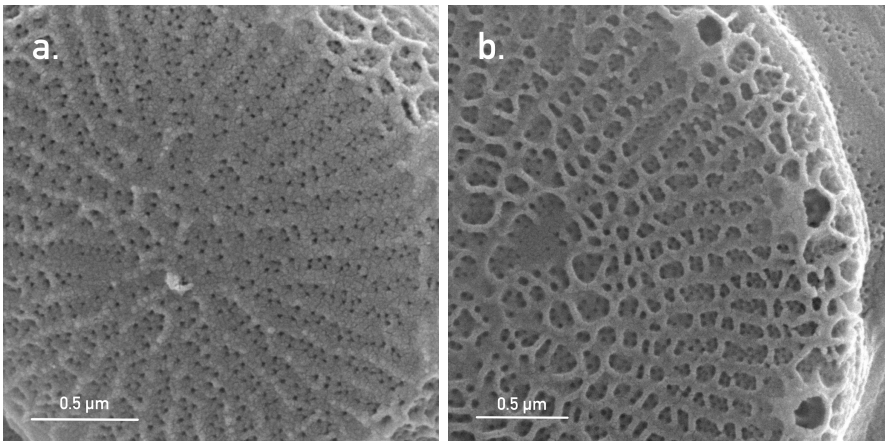

Figure 4.18: SEM of the effects of the microfilament inhibitor cytochalasin D on valve structure. (a) The ribs and cross-links do not protrude from the valve surface, and there is no central fultoportulae. (b) The fultoportulae are open, and not that extended from the valve.

The mean number of rimoportulae were not changed significantly for any of the inhibitors. A summary of some of the measurable features of the valve is given in Table 4.3. In most of the frustules, regardless of treatment, there was also observed relatively open rimoportulae, as seen in Figure 4.18b.

Table 4.3: Statistical representation of features of the inhibitor-treated valves. The number of valves that were observed to have an irregular number of fultoportulae, and the number of valves counted in total. The mean number of rimoportulae was counted for each of the inhibitors and the control.

Inhibitor	Several fultoportulae	No fultoportula	No. of rimoportulae
Colchicine	4/17	2/17	10.1
Oryzalin	0/16	3/16	10.8
Cytochalasin D	0/13	5/13	10.7
Control	0/17	0/17	10.1

4.7.3 The effect of cytoskeleton inhibitors on culture growth

The cultures treated with cytoskeleton inhibitors were analysed in a flow cytometer before treatment, and 4 days after. This was done in order to confirm if the cultures had decreased growth. The cell density is presented in Table 4.4. In addition, the fraction of live cells are given for the treated cultures. The cytochalasin D- and colchicine-treated cultures had a significantly lower cell density and a lower fraction of live cells after the 4-day treatment compared to the oryzalin-treated culture and the control.

Table 4.4: The cell density of each culture of *T. pseudonana* before and 4 days after addition of cytoskeleton inhibitors. The four cultures were derived from a common start culture, which is why they have the same cell density at the beginning of the experiment. The fraction of alive cells for the 4 day-culture is also given.

	Before addition	4 days after addition	
Inhibitor	Cell density [cells/µl]	Cell density [cells/µl]	Fraction of alive cells
Colchicine	744	2 408	24 %
Oryzalin	744	3 273	33 %
Cytochalasin D	744	1 987	20 %
No inhibitor	744	3 554	35 %

5 Discussion

5.1 Synchronisation experiments

The first synchronisation experiment was ended prematurely, as some of the fluorescence measurements were exceptionally high (Figure 4.3). The 0h and 2h measurements between 100 000 and 400 000 fu, where the wild-type had the highest. In a similar experiment by Gresseth (2019) the fluorescence measured by the same transformants were approximately 14 000 fu at the highest expression during a synchronisation experiment (see Appendix E. Because of this divergence, it was deemed improbable that the measurements represented the actual fluorescence of the cells, and they were discarded as faulty equipment. The second synchronisation experiment was also discarded (Figure 4.4). It is improbable for the cell density to increase by 30 % in an hour, and then that the equal amount of cells dies in the hour after. It is all the more unlikely that this were to happen three times during the course of only 7 hours. The fluorescence of the cells did not change significantly during the course of the experiment either. Because of both of these unexpected results, it was assumed that faulty equipment was responsible. In hindsight, the stable fluorescence could be explained by lack of expression of the mNeonGreen-Tp24711 protein by the transformants.

In retrospect, the results from the third synchronisation experiment make sense, although it was assumed to be faulty data at the time (Figure 4.5). The experiment was done in advance of the realisation that the cells had stopped expressing the mNeonGreen-Tp24711 protein, which is why the fluorescence measurements were assumed faulty. There was some change in fluorescence during the course of the experiment, but this could be due to natural changes in the cells' autofluorescence. The fluorescence anyway wasn't similar to what has been seen in previous successful synchronisation experiments studying the mNeonGreen-Tp24711 expression (Appendix E). This previous experiment showed that the Tp24711 gene is highly expressed during the G2+M phase, and a lower expression during the rest of the cell cycle. In this experiment there was on the contrary a small increase in expression during G1.

In the cell cycle determination (Figure 4.6), it was initially difficult to conclude anything about the cell cycle from the results. The cell cycle was expected to progress from G1 to S to G2+M, but this was not the case for either of the cultures. If one looks at only the G2+M, however, the progression adds up with the progression of the cell divisions (as seen by change in cell density). For the Tp24711-1.2 culture some of the cells were seen to go out of G2+M at the beginning of the experiment, yielding an

increase in cell density in the first hour (Figure 4.5a). Then again, an after the cells exited G2+M at 6-8 hours, an increase in cell density was seen at the 8h mark. The same was observed for the Tp24711-1.5 transformants, as they had cells leaving G2+M 2-3 hours after Si addition, and then an increase in cell density was seen at 3 hours. The second peak in in G2+M of the Tp24711-1.5 transformants and the peak of the wild-type were both on their way down at the end of the experiment, so an increase in cell density would have been expected for both of them if the experiment had run longer.

The G1 and S phases did not show a pattern for neither of the cultures during the cell cycle determination. This observation could be explained looking at Figure 4.7a. Here, the G1 and S phase of the cells are overlapping considerably, which makes them hard to distinguish. The NovoExpress® software has (to the extent of the authors knowledge) not been known to be used on diatoms before. It is therefore possible that it wasn't calibrated for those types of cells, and thus had difficulty telling the two phases apart for this particular type of species. It is also possible that the software could have predicted more easily if it had been set to count more events. In addition, the software expected the user to fit the gating of the cells in Figure 4.7b, but it was hard to work with, as it was particular about how the gate was set in order for it to calculate the amount in each stage. This made the gates look differently for each of the samples, which could have excluded some cells that should have been included and vice versa.

5.2 Expression of mNeonGreen-Tp24711

There was comprehensive evidence that mNeonGreen-Tp24711 was not expressed in the transformants. First, all images of the transformants in both fluorescence microscopy and confocal microscopy showed no sign of fluorescence outside of the autofluorescence emitted from the chloroplasts (Figures 4.10 and 4.11), with the exception of the last images of the Tp24711-1 transformants (Figures 4.8 and 4.9). Second, the western blot showed no sign of expression of the mNeonGreen-Tp24711 fusion protein (Figure 4.12). Third, the overall fluorescence in the attempted synchronisation experiments (Figures 4.3, 4.4 and 4.5) was small in comparison with what was seen in a previous synchronisation experiment with the same transformants (see Appendix E). The previous study showed a fluorescence between 6 000 and 14 000 fu for the transformants throughout the cell cycle, but these new experiments show a fluorescence of 4 000 fu at the most (with the exception of the extreme data observed in the first synchronisation experiment).

In the western blot, only the pelleted positive control showed signs of expression (Figure 4.12). Two bands were visible, which often is seen due to

degradation of the protein. In order to get an accurate result, antibodies for the ladder should have been used. Since these antibodies weren't used, the size of the bands could only be estimated. The mNeonGreen protein should be 26.7 kDa, so it can be assumed that the largest band (of approximately 25 kDa) from the blot is the actual mNeonGreen protein. Since no bands were seen for either of the transformants, pelleted or not, it can be assumed that the transformants didn't produce significant amounts of the protein.

A possible explanation for the non-fluorescent transformants is that it was a response to stressful conditions. The Tp24711-1 transformants went through a period without nourishment before the experiments started (Tore Brembu, personal communications, 25.06.20), and for both the Tp24711-2 and Tp24711-3 transformants there was a somewhat slow progression in the process after the clones were picked before they were fed. For the Tp24711-2 transformants, the clones were cultivated in wells for 34 days without additional feeding, which is a significant amount of time considering they are usually fed twice a week. This stress could have caused the cells to silence genes, whereas the mNeonGreen-Tp24711 could be one of them. The Tp24711-1 cells did not express the mNeonGreen-Tp24711 protein for approximately 4 months, which makes it likely that the gene silencing was something more permanent than e.g. transcriptional or translational regulation. The gene is therefore assumed to have been regulated through epigenetic mechanisms, as diatoms are known to make epigenetic change in response to stress-factors (Tirichine and Bowler, 2011). Previous studies of the Tp24711 gene by Gresseth (2019) showed an expression similar to what was seen after the transformants regained their mNeonGreen fluorescence (see Appendix E), which indicated that the mechanism of silencing was reversible. What makes these cells remarkable is that the same regulation seems to have happened for all of the transformants, assuming that the Tp24711-2 and Tp24711-3 transformants also would have regained their expression under the same conditions. Since it happened to all of them, it could be because the Tp24711 gene itself or its promoter is prone to regulation. It may indicate that the gene is not vital, seeing as non-essential genes are not prioritised in times of stress (Teng et al., 2013). The fact that the Tp24711-1 transformants regained their fluorescence could be due to either the cold storage of the cells, or perhaps they only needed time undo the regulation.

PCR of the Tp24711-2 transformants yielded several bands, which suggests that the primers bound non-specifically to the template (Figure 2.2). The bands of interest were identified by comparing them with wild-type control. Non-specific binding is often caused by a low annealing temperature, which is assumed to be the cause in this experiment. The calculation of the annealing temperature was done in a software provided by the producer

of the Taq polymerase, and the temperature should generally be trusted. Other users of the same kit and software have, however, experienced similar non-specific binding (Marthe Hafskjold, personal communications, 23.06.20), and it is therefore assumed that the software underestimates the necessary annealing temperature.

The observed size of the PCR fragments differed from the expected size for all of the fragments, which could be caused by insertions or deletions in the segments. As previously discussed, it is not likely that the non-fluorescence in Tp24711-1 is caused by deletions, insertions or any other permanent change, as the mNeonGreen fluorescence returned. It can not be stated with certainty that the non-fluorescence is caused by the same factors for the Tp24711-2 transformants as for the Tp24711-1 transformants, as the mNeonGreen fluorescence has yet to return to the Tp24711-2 transformants. It is however a certain probability of them having the same cause, as the mNeonGreen fluorescence was observed lost for all three generations of transformants after similar stressful conditions. It is also probable that the size of bands in the PCR can be discarded as faulty reaction conditions. The PCR can therefore neither confirm nor reject that the plasmid insert sequence has been altered. The experiment could easily have been repeated with a higher annealing temperature, had it not been for the lack of time at the end of the thesis. This could have helped identify or rule out what happened to the plasmid insert.

5.3 Effect of cytoskeleton inhibitors on frustule morphology

Both of the microtubule inhibitors caused an overgrowth of the ribs and cross-links (Figures 4.16 and 4.17). The surface looked like a tangled web, which could result from a lack of organised placements by the microtubules. According to Tesson and Hildebrand (2010b), the microtubules should be involved in positioning of structures in several diatom species. In some of the oryzalin-treated frustules it was also seen a lack of nanopores. They could just be hidden from view due to the overgrowth of ribs and cross-links, or maybe the overgrowth affected not only the ribs and cross-links, but also the entire surface of the valve. For a couple of the colchicine-treated cells it was also seen a lack of cross-links and ribs, which seems contradictory to the other overgrown frustules from the same treatment. It is not understood how the same inhibitor can affect the frustule morphology in such conflicting ways, but it is at least evident that it is involved in the placement or production of the ribs and cross-links. In *C. cryptica* the colchicine and oryzalin-treated

cells had a misalignement in placement of the ribs (Tesson and Hildebrand, 2010a), which was not observed in *T. pseudonana*. This difference could suggest that the microtubules have different roles in different species.

Some of the colchicine-treated cells had more than one fultoportulae (Figure 4.16a), which may indicate that the microtubules are take part in placement of the fultoportulae. It has previously been suggested that organic complexes are involved in deterring silification where the portulae are (Tesson and Hildebrand, 2010a), and so the microtubules could be involved in positioning of these. When the microtubules don't support these molecules, they may not be placed as usual, which could lead a different positioning of the fultoportulae. On the other hand, several of the colchicine- and oryzaline-treated frustules lacked a central fultoportulae (Table 4.3). The different phenotypes could be explained by an inconsistency in how the inhibitors affect the valve, as was discussed in the last paragraph. It is anyway evident that the microtubules affect the production of the fultoportulae. The ones that were produced did not deviate from the control phenotype, which means that the microtubules are likely involved in whether or not the fultoportulae is produced, but not in formation itself.

The oryzalin-treated cells did not show as much of a phenotype overall compared to the colchicine-treated ones. This could be due to several causes, but it is likely that the concentration of the inhibitor was not high enough during treatment. After the treatment it was observed that the oryzalin-treated culture had almost the same density of cells as the wild-type control culture, which was higher than both the colchicine and cytochalasin D-treated cultures (Table 4.4). In addition, they were seen to have a fraction of live cells that was more similar to that of the wild-type control culture than the colchicine- and cytochalasin D-treated cultures. The experiment using oryzalin should be repeated with a higher concentration, in order to see if it would yield a clearer phenotype.

Several of the cytochalasin D-inhibited cells lacked ribs and cross-links, leaving only remnants of the mesoscale structures behind as a rough surface (Figure 4.18a). In Tesson and Hildebrand (2010b) it was proposed that the microfilaments are responsible in patterning of the valve on a mesoscale, which could explain this observed morphology. Additional experiments in Tesson and Hildebrand (2010a) showed that the normally raised pore fields of *C. cryptica* did not protrude from the surface of the valve after treatment with cytochalasin D. The flat ribs and cross-links of *T. pseudonana* could be caused by the same mechanism. In studies where the function of Sin-1 was knocked out, it was seen that the cross-links of the valve were missing (Förlich et al., 2019). Assuming that the silicanins have a similar role in frustule synthesis, the combined results of the experiment with Sin-1 and

these inhibitor-treated cells is in accordance with the hypothesis that the cytoskeleton and silicanins are connected somehow.

Another observed phenotype of the microfilament-inhibited cells is that the central fultoportulae is missing (Figure 4.18a). In Tesson and Hildebrand (2010a) it was suggested that microfilaments are involved in patterning of the mesoscale structures. Continuing this argument, the cells are simply unable to form the fultoportulae in the absence of microfilaments. If this is true, it seems that microtubules decide where and if the fultoportulae are made, while the microfilaments make the fultoportulae.

The findings of the inhibitor experiment are somewhat limited. First, it is possible that the frustules of the most affected cells were broken by the harsh treatment of the frustule cleaning. Many frustules survived the procedure, but it is likely that those were the ones that had the least amount of phenotype as inhibitors are expected to make the frustule more fragile. This would further make the procedure select for the least affected frustules. Second, the results may differ within each inhibitor-treatment, if the cells were in different stages of the cell cycle at the beginning of the treatment. Some of the frustule may have been in the beginning of their frustule synthesis, while others were almost finished at the addition of inhibitor. Addition at the different cell stages could yield different morphologies, with no definite way of knowing how this affected the outcome of the results. Third, the procedure of cleaning may have affected the frustule morphologies. For instance, several of the studied valves had more open and broken fulto- and rimoportulae than what has been observed in other articles (Gröger et al., 2016), as seen in e.g. Figure 4.18b. This may be due to the inhibitors, but because it was also observed in the control it is more likely that this is caused by the procedure or a local phenotype within the culture. Lastly, the experiment chose to focus on the morphology of the valves rather than the girdle bands. Both microfilaments and microtubules have been seen to be located near the girdle bands, and so they are likely also involved in the synthesis of these (Tesson and Hildebrand, 2010b). In addition, a previous study of Tp24711 showed that the protein is located in the girdle bands SDV, and so if the cytoskeleton and the silicanin are connected this could also be an interesting subject of research in the future.

5.4 Future prospects

This thesis failed to find any new information about the expression of Tp24711 in *T. pseudonana*, thus a lot is yet to be discovered about the protein. For future research, more studies of expression of the protein using cell cycle determination and western blot analysis could be done. The synchron-

ised cells could also be studied in a confocal microscope to identify how the intracellular location changes during the course of the cell cycle, similarly to what has been done with Sin-1 by Kotzsch et al. (2017). A microscopy experiment using cytoskeleton inhibitors and mNeonGreen-Tp24711 transformants could yield information about how the inhibitors affect the intracellular location of the fluorescent protein, and therefore if the cytoskeleton is connected to Tp24711. To develop a full picture of the protein's role in frustule morphology, CRISPR technology could be used to knock out the gene such has already been done in Sin-1 (Förlich et al., 2019). Studying how the knockout affects the growth and the mechanical strength of the cells and the morphology of the frustule could thereby indicate the role of the protein.

Several silicanins have been discovered (Brembu et al., 2017), but have yet to be studied. By comparing the different silicanins in several experiments it can be decided if they their functions are similar or complementary. As the cross-links disappeared in knock-out experiments of only Sin-1 (Förlich et al., 2019), it is possible that they are all decisive for the normal phenotype in their own way. Silicanins have been found in ditantly related diatoms, thus the silicanins from the same subfamilies could be compared to see how they act in different species. The silicanins are also suspected to connect the cytoskeletal network with the frustule during silica polymerisation, and so further research should investigate whether this is true. By adding cytoskeleton inhibitors to cultures of fluorescent transformants such as mNeonGreen-Tp24711, it could be observed whether or not absence of the cytoskeleton affects the intracellular position of the silicanin. This experiment could also be useful to repeat with another protein family suspected to be involved in communication across the silicalemma – SAP.

There are many proteins that are thought to be involved in silica polymerisation that are yet to be characterised, such as the ones discovered in Brembu et al. (2017). Several of the proteins identified in this article had KXXK-domains, which would be interesting to characterise further, as these domains are thought to take part in silica polymerisation in silaffins and cingulins. As CRISPR technology becomes more accessible, it will also be easier to investigate the implications of removing the function of the individual genes. A recent study has also developed a method using Artificial Neural Networks to detect changes in diatom strains that may be indistinguishable to the naked eye (Trofimov et al., 2019). This method could be used in future knock-out experiments on frustule-associated proteins in order to determine their function in frustule formation, which could lead to discoveries that would have otherwise been improbable.

6 Conclusion

The mNeonGreen-fluorescence was apparently lost from the *T. pseudonana* cells for the majority of the experiments, which was confirmed through microscopy, flow cytometry and western blotting. As the phenotype was only transient for the Tp24711-1 transformants, the cause of the missing fluorescence was thought to be epigenetics brought by stress as a result of starvation. The Tp24711-2 and Tp24711-3 transformants never regained their mNeonGreen fluorescence, but it may be speculated that they too would express mNeonGreen fluorescence given time and proper care. A PCR was run to analyse the insert of the pTpPuc3-Tp24711-mNeonGreen plasmid, which was inconclusive.

In the cytoskeleton inhibitor experiment. The two microtubule inhibitors (colchicine and oryzalin) resulted in ribs and cross-links that were grown in a more unstructured manner, although some of the colchicine-treated frustules also lacked ribs and cross-links almost completely. These are two contradictory observations, but still, it is evident that the microtubules are involved in the process of rib and cross-link development. The oryzalin-treated frustules had some phenotype, but to a less degree than the colchicine-treated frustules, which was thought to be due to a low concentration of the inhibitor. It is therefore recommended that the experiment is repeated with a higher concentration of oryzalin. The microfilament inhibitors affected the cells by a lack of protrusion in the ribs and cross-links, and so the microfilaments were suggested to take part in formation of these particular mesoscale structures. In previous studies in *C. cryptica* it was suggested that the microtubules are involved in positioning of structures, while microfilaments are involved in patterning of the surface. If this is the case also in *T. pseudonana*, it was suggested that the microtubules are involved in deciding where and if the fultoportulae get made, and the microfilaments participate in the formation of the fultoportulae.

This study did not yield any new information about the function or expression of Tp24711 in *T. pseudonana*, so for further work it would be interesting to do knock-outs of the gene to see how it would affect the functionality and the morphology of the frustule. New inhibitor experiments could be done on the mNeonGreen-Tp24711 transformants to see how the loss of the cytoskeleton affects the intracellular location of the protein. Previous experiments have also found several proteins expected to take part in frustule formation, and these should be studied in further detail using methods such as knock-outs, transcriptomics and fusion proteins. At this time there is still a lot yet to be discovered about frustule formation, but every investigated molecule leads one step closer to understanding this complex process.

References

Ambrust, E.V. (2009). 'The life of diatoms in the world's oceans'. *Nature* 459 (7244), 185–192.

Armbrust, E. et al. (2004). 'The Genome of the Diatom *Thalassiosira pseudonana*: Ecology, Evolution, and Metabolism'. *Science* 306 (5693), 79–86.

Bidle, K.D. and F. Azam (1999). 'Accelerated dissolution of diatom silica by marine bacterial assemblages'. *Nature* 397, 508–512.

Bowler, C., A. Vardi and A. Allen (2010). 'Oceanographic and Biogeochemical Insights from Diatom Genomes'. *Annual Review of Marine Science* 2 (1), 333–365.

Brembu, T. et al. (2017). 'Dynamic responses to silicon in *Thalasiossira pseudonana* - Identification, characterisation and classification of signature genes and their corresponding protein motifs'. *Scientific Reports* 7 (1), 4865.

Brunner, E. et al. (2009). 'Chitin-based organic networks: An integral part of cell wall biosilica in the diatom *Thalassiosira pseudonana*'. *Angewandte Chemie - International Edition* 48 (51), 9724–9727.

Davis, A.K., M. Hildebrand and B. Palenik (2005). 'A stress-induced protein associated with the girdle band region of the diatom *Thalassiosira pseudonana* (Bacillariophyta)'. *Journal of Phycology* 41 (3), 577–589.

De Sanctis, S. et al. (2016). 'PSCD Domains of Pleuralin-1 from the Diatom *Cylindrotheca fusiformis*: NMR Structures and Interactions with Other Biosilica-Associated Proteins'. *Structure* 24 (7), 1178–1191.

De Tommasi, E., J. Gielis and A. Rogato (2017). 'Diatom Frustule Morphogenesis and Function: a Multidisciplinary Survey'. *Marine Genomics* 35, 1–18.

Durkin, C.A., T. Mock and E.V. Armbrust (2009). 'Chitin in diatoms and its association with the cell wall'. *Eukaryotic Cell* 8 (7), 1038–1050.

Ehrlich, H. (2010). 'Chitin and collagen as universal and alternative templates in biomineralization'. *International Geology Review* 52 (7), 661–699.

Falciatore, A. and C. Bowler (2002). 'Revealing the molecular secrets of marine diatoms'. *Annual Review of Plant Biology* 53, 109–130.

Finkel, Z. and B. Kotrc (2010). 'Silica Use Through Time: Macroevolutionary Change in the Morphology of the Diatom Frustule'. *Geomicrobiology Journal - GEOMICROBIOL J* 27 (6), 596–608.

Förlich, S. et al. (2019). 'Control of biosilica morphology and mechanical performance by the conserved diatom gene Silicanin-1'. *Communications Biology* 2 (245).

Fuhrmann-Lieker, T. et al. (2004). 'Diatoms as living photonic crystals'. *Applied Physics B* 78 (3), 257–260.

Gresseth, M. (Dec. 2019). *Functional studies of silicanin Tp24711 in diatom cell wall biomineralisation*. Project thesis in TBT4500. Department of Biotechnology and Food Science, Norwegian University of Science and Technology.

Gröger, P. et al. (2016). 'Establishing super-resolution imaging for proteins in diatom biosilica'. *Scientific Reports* 6, 36824.

Hamm, C.E. et al. (2003). 'Architecture and material properties of diatom shells provide effective mechanical protection'. *Nature* 421 (6925), 841–843.

Hardin, J., G. Bertoni and L.J. Kleinsmith (2017). 'Cytoskeletal systems'. In: *Becker's world of the cell*. 9th ed. Pearson Education Limited, pp. 375–400.

Hildebrand, M., L.G. Frigeri and A.K. Davis (2007). 'Synchronized growth of *Thalassiosira pseudonana* (Bacillariophyceae) provides novel insights into cell-wall synthesis processes in relation to the cell cycle'. *Journal of Phycology* 43 (4), 730–740.

Hildebrand, M., S.J. Lerch and R.P. Shrestha (2018). 'Understanding Diatom Cell Wall Silicification — Moving Forward'. *Frontiers in Marine Science* 5 (125), 1–19.

Hildebrand, M. et al. (2006). 'Nanoscale control of silica morphology and three-dimensional structure during diatom cell wall formation'. *Journal of Materials Research* 21 (10), 2689–2698.

Karas, B.J. et al. (2015). 'Designer diatom episomes delivered by bacterial conjugation'. *Nature Communications* 6 (1), 6925.

Kirkham, A.R. et al. (2017). 'A role for the cell-wall protein silacidin in cell size of the diatom *Thalassiosira pseudonana*'. *ISME Journal* 11 (11), 2452–2464.

Kotzsch, A. et al. (2016). 'Biochemical Composition and Assembly of Biosilica-associated Insoluble Organic Matrices from the Diatom *Thalassiosira pseudonana*'. *The Journal of Biological Chemistry* 291 (10), 4982–4997.

Kotzsch, A. et al. (2017). 'Silicanin-1 is a conserved diatom membrane protein involved in silica biomineralization'. *BMC Biology* 15 (1), 65.

Kröger, N., C. Bergsdorf and M. Sumper (1994). 'A new calcium binding glycoprotein family constitutes a major diatom cell wall component.' *The EMBO Journal* 13 (19), 4676–4683.

Kröger, N., C. Bergsdorf and M. Sumper (1996). 'Frustulins: Domain conservation in a protein family associated with diatom cell walls'. 239 (2), 259–264.

Kröger, N., R. Deutzmann and M. Sumper (1999). 'Polycationic peptides from diatom biosilica that direct silica nanosphere formation'. *Science* 286 (5442), 1129–1132.

Kröger, N. and N. Poulsen (2008). 'Diatoms—From Cell Wall Biogenesis to Nanotechnology'. *Annual Review of Genetics* 42 (1), 83–107.

Kröger, N. and R. Wetherbee (2000). 'Pleuralins are involved in theca differentiation in the diatom *Cylindrotheca fusiformis*'. *Protist* 151 (3), 263–273.

Kröger, N. et al. (1997). 'Characterization of a 200-kDa diatom protein that is specifically associated with a silica-based substructure of the cell wall'. *European Journal of Biochemistry* 250 (1), 99–105.

Kröger, N. et al. (2000). 'Species-specific polyamines from diatoms control silica morphology'. *Proceedings of the National Academy of Sciences of the United States of America* 97 (26), 14133–14138.

Kröger, N. et al. (2002). 'Self-assembly of highly phosphorylated silaffins and their function in biosilica morphogenesis'. *Science* 298 (5593), 584–586.

Lechner, C.C. and C.F.W. Becker (2015). 'Silaffins in silica biomineralization and biomimetic silica precipitation'. *Marine Drugs* 13 (8), 5297–5333.

Li, Y. et al. (2016). 'Chitinase producing bacteria with direct algicidal activity on marine diatoms'. *Scientific Reports* 6, 21984.

Losic, Dusan et al. (2006). 'Pore Architecture of Diatom Frustules: Potential Nanostructured Membranes for Molecular and Particle Separations'. *Journal of Nanoscience and Nanotechnology* 6 (4), 982–989.

Morrissette, N.S. et al. (2004). 'Dinitroanilines Bind α-Tubulin to Disrupt Microtubules'. *Molecular Biology of the Cell* 15 (4), 1960–1968.

Nymark, M. et al. (2019). 'Loss of ALBINO3b Insertase Results in Truncated Light-Harvesting Antenna in Diatoms'. *Plant physiology* 181 (3), 1257–1276.

Poulsen, N., M. Sumper and N. Kröger (2003). 'Biosilica formation in diatoms: Characterization of native silaffin-2 and its role in silica morphogenesis'. *Proceedings of the National Academy of Sciences of the United States of America* 100 (21), 12075–12080.

Rabinovitch, P. (1993). *Introduction to cell cycle analysis*. Pheonix Flow Systems Inc. San Diego, CA. USA.

Raven, J.A. and A. Waite (2004). 'The evolution of silicification in diatoms: Inescapable sinking and sinking as escape?' *New Phytologist* 162 (1), 45–61.

Richthammer, P. et al. (2011). 'Biomineralization in Diatoms: The Role of Silacidins'. *ChemBioChem* 12 (9), 1362–1366.

Robinson, D.H. and C.W. Sullivan (1987). 'How do diatoms make silicon biominerals?' *Trends in Biochemical Sciences* 12, 151–154.

Romann, J. et al. (2016). 'Diatom frustules as a biomaterial: effects of chemical treatment on organic material removal and mechanical properties in cleaned frustules from two *Coscinodiscus* species'. *Journal of Porous Materials* 23 (4).

Scheffel, A. et al. (2011). 'Nanopatterned protein microrings from a diatom that direct silica morphogenesis'. *Proceedings of the National Academy of Sciences of the United States of America* 108 (8), 3175–3180.

Shah, M.A. and A.A. Khan (2014). 'Use of diatomaceous earth for the management of stored-product pests'. *International Journal of Pest Management* 60 (2), 100–113.

Shrestha, R.P., B. Tesson and T. Norden-Krichmar (2012). 'Whole transcriptome analysis of the silicon response of the diatom *Thalassiosira pseudonana*'. *BMC Genomics* 13 (1), 499.

Strand, T. et al. (2014). 'A New and Improved Host-Independent Plasmid System for RK2-Based Conjugal Transfer'. *PloS one* 9 (3), 90372.

Sumper, M. (2002). 'A phase separation model for the nanopatterning of diatom biosilica'. *Science* 295 (5564), 2430–2433.

Sumper, M. (2004). 'Biomimetic patterning of silica by long-chain polyamines'. *Angewandte Chemie - International Edition* 43 (17), 2251–2254.

Sumper, M. and E. Brunner (2006). 'Learning from diatoms: Nature's tools for the production of nanostructured silica'. *Advanced Functional Materials* 16 (1), 17–26.

Teng, X. et al. (2013). 'Genome-wide consequences of deleting any single gene'. *Molecular cell* 52 (4), 485–494.

Tesson, B. and M. Hildebrand (2010a). 'Dynamics of silica cell wall morphogenesis in the diatom *Cyclotella cryptica*: Substructure formation and the role of microfilaments'. *Journal of Structural Biology* 169 (1), 62–74.

Tesson, B. and M. Hildebrand (2010b). 'Extensive and intimate association of the cytoskeleton with forming silica in diatoms: Control over patterning on the meso- and micro-scale'. *PLoS ONE* 5 (12), 14300.

Tesson, B., S.J. Lerch and M. Hildebrand (2017). 'Characterization of a New Protein Family Associated With the Silica Deposition Vesicle Membrane Enables Genetic Manipulation of Diatom Silica'. *Scientific Reports* 7 (1), 13457.

Tirichine, L. and C. Bowler (2011). 'Decoding algal genomes: tracing back the history of photosynthetic life on Earth'. *Plant J* 66 (1), 45–57.

Traller, J.C. and M. Hildebrand (2013). 'High throughput imaging to the diatom *Cyclotella cryptica* demonstrates substantial cell-to-cell variability in the rate and extent of triacylglycerol accumulation'. *Algal Research* 2 (3), 244–252.

Trofimov, A.A. et al. (2019). 'Deep data analytics for genetic engineering of diatoms linking genotype to phenotype via machine learning'. *npj Computational Materials* 5 (1), 67.

van de Poll, W.H., E.G. Vrieling and W.W.C. Gieskes (1999). 'Location and Expression of Frustulins in the Pennate Diatoms *Cylindrotheca Fusiformis*, *Navicula Pelliculosa*, and *Navicula Salinarum* (Bacillariophyceae)'. *Journal of Phycology* 35 (5), 1044–1053.

Vrieling, E.G. et al. (1999). 'Diatom silicon biomineralization as an inspirational source of new approaches to silica production'. *Journal of Biotechnology* 70 (1-3), 39–51.

Wan, Y. and D. Zhao (2007). 'On the controllable soft-templating approach to mesoporous silicates'. *Chem Rev.* 107 (7), 2821–2860.

Wenzl, S. et al. (2008). 'Silacidins: Highly acidic phosphopeptides from diatom shells assist in silica precipitation *in vitro*'. *Angewandte Chemie - International Edition* 47 (9), 1729–1732.

Yang, W., P.J. Lopez and G. Rosengarten (2011). 'Diatoms: Self assembled silica nanostructures, and templates for biochemical sensors and biomimetic membranes'. *Analyst* 136 (1), 42–53.

A Media

A.1 f/2-medium

The required ingredients for f/2-medium is given in Tab A.1. All nutrients are mixed together, and sterile filtered (2 µm). Autoclave the filtered sea water, and add the filtered nutrients. For Si-free f/2-medium, do not add Na_2SiO_3 x $9H_2O$.

Table A.1: The ingredients required to make 1 l f/2-medium.

1 ml	$NaNO_3$ (stock)
1 ml	NaH_2PO_4 x H_2O (stock)
1 ml	Na_2SiO_3 x $9H_2O$
0.5 ml	Vitamins (stock)
1 ml	Trace metals (stock)
1 l	Filtered sea water (0.2 µm sterile filter)

A.2 LB-medium

The recipe for the LB-medium is given in Table A.2. Mix all the ingredients and autoclave.

Table A.2: The ingredients required to make 1 l LB-medium.

5 g	Tryptone
5 g	NaCl
7.5 g	Yeast extract
1 l	Purified water

A.3 SOC-medium

The recipe for SOC-medium is given in Table A.3. Add tryptone, NaCl and yeast extract to 950 ml of deionised water. Shake until all of the ingredients have been dissolved, and add KCl. Adjust pH to 7.0 using 5 M NaOH. Add deionised water to a total volume of 1 l. Autoclave and add 5 ml of sterile filtered 2 M $MgCl_2$ and a 1 M solution of glucose (sterile).

Table A.3: The ingredients required to make 1 l SOC-medium.

20 g	Tryptone
0.5 g	NaCl
5 g	Yeast extract
950 ml	Deionised water
10 ml	250 mM KCl
X ml	5 M NaOH
40-X ml	Deionised water
5 ml	2 M $MgCl_2$
20 mL	1 M Glucose

A.4 L1-medium

The recipe for L1-medium is given in Table A.4. All nutrients are mixed together, and sterile filtered (2 µm). Autoclave the filtered sea water, and add the filtered nutrients. For Si-free f/2-medium, do not add Na_2SiO_3 x $9H_2O$.

Table A.4: The ingredients required to make 1 l L1-medium.

4.36 g	Na_2EDTA x $2H_2O$
3.15 g	$FeCl_3$ x $6H_2O$
1 ml	178.10 g/l $MnCl_2$ x H_2O
1 ml	23.00 g/l $ZnSO_4$ x $7H_2O$
1 ml	11.90 g/l $CoCl_2$ x $6H_2O$
1 ml	2.50 g/l $CuSO_4$ x $5H_2O$
1 ml	19.9 g/l Na_2MoO_4 x $2H_2O$
1 ml	1.29 g/l H_2SeO_3
1 ml	2.63 g/l $NiSO_4$ x $6H_2O$
1 ml	1.84 g/l Na_3VO_4
1 ml	1.94 g/l K_2CrO_4
950 ml	Filtered sea water

B Protein concentration of protein isolate

When the proteins were isolated from the transformant and wild-type cultures, the concentration was measured using Qubit Fluorometric Quantification from Thermo Scientific. The protein concentration was measured as shown in Table B.1. The protein isolate was used further in a western blot.

Table B.1: The concentration of the protein isolate from wild-type and the two cultures of the Tp24711-1 transformants.

Source of protein isolate	Concentration [µg/ml]
TpWt	308
Tp24711-1.2	480
Tp24711-1.5	326

C Protocols

C.1 SDS-PAGE gel

To make the two gels (12 % acrylamide) for SDS-PAGE, two types of gel needed to be prepared; the resolving gel and the stacking gel. The recipes are given in Table C.1. First, a layer of resolving gel was added to the mini gel tank, and then a layer of stacking gel. The chamber was filled with 1X NuPAGE^{TM} MOPS SDS running buffer from Invitrogen^{TM}. The Precision Plus Protein^{TM} Dual Color Standards was used as a ladder for the gel.

Table C.1: The recipe for resolving gel and stacking gel in SDS-PAGE. SDS = sodium dodecyl sulfate; APS = ammonium persulfate; TEMED = Tetramethylethylenediamine.

Resolving gel [µl]	Stacking gel volume [µl]	Component
6 300	4 300	dH_2O
4 500	704	40 % acrylamide
3 900	-	1.5 Tris
-	1 820	0.5 Tris
150	70	10 % SDS
150	70	APS
15	15	TEMED

C.2 iBind^{TM} solution

The recipe for the iBind^{TM} solution used for the western blot is given in Table C.2. The buffer and additive was provided from Thermo Scientific.

Table C.2: The recipe for the iBind solution from Thermo Scientific.

500 µl	iBind^{TM} Flex 100X Additive
10 ml	iBind^{TM} Flex 5X Buffer
39.5 ml	MQ water

C.3 DNeasy plant pro kit

The following is the protocol of the DNeasy® plant pro kit from Qiagen that was followed for DNA-isolation.

1. Add 1 ml of the cell culture to a 2 ml tissue disruption tube.

2. Place samples in the TissueLyser and run for 2 minutes at 24 Hz. Reorient the adapter, and run for 2 new minutes at 24 Hz.

3. Transfer the supernatant to a new 1.5 ml microcentrifuge tube, and add 200 µl of CD2 solution (provided). Vortex for 5 seconds.

4. Centrifuge at 12 000 g for 1 minute and transfer the supernatant to a new 1.5 ml microcentrifuge tube.

5. Add 500 µl of APP buffer (provided) and cortex for 5 seconds.

6. Load 600 µl of the lysate onto a MB spin column and centrifuge for 1 minute at 12 000 g.

7. Discard the flow-through and repeat step 6.

8. Place the spin column onto a new 2 ml collection tube and add 650 µl of AW1 buffer (provided).

9. Centrifuge for 1 minute at 12 000 g, and discard the flow-through. Place the spin column back on the same collection tube.

10. Add 650 µl of AW2 buffer (provided) to the spin column and centrifuge for 1 minute at 12 000 g. Place the spin column back onto the same collection tube.

11. Centrifuge for 2 minutes at 16 000 g, and place the spin column into a new 1.5 ml collection tube.

12. Add 100 µl of EB buffer (provided) to the centre of the white filter membrane, and centrifuge for 1 minute at 12 000 g. Discard the spin colum

C.4 PCR reaction conditions

The recipe in the protocol for the Phusion® High-Fidelity DNA polymerase from New England Biolabs® is given in Table C.3. The mixture was prepared on ice, with addition of the DNA polymerase in the end.

Table C.3: The recipe for the reaction solution of the Phusion® High-Fidelity DNA polymerase from New England Biolabs®.

30 µl	ddH_2O
10 µl	5X Phusion HF Buffer
1 µl	10 mM dNTP
2.5 µl	Forward primer
2.5 µl	Reverse primer
2 µl	Template DNA
1.5 µl	DMSO
0.5 µl	Phusion DNA polymerase

The reaction conditions for the PCR is given in Table C.4. The annealing temperature was calculated using a T_m-calculator provided by New England Biolabs® (`tmcalculator.neb.com`).

Table C.4: The settings on the PCR machine for all the investigated fragments of the mNeonGreen-Tp24711-pTpPuc3 plasmid. The annealing temperature and extension time differed for each fragment, and is given in the following order: partial fusion gene, whole fusion gene, silicanin

Process	Temperature [°C]	Time [s]
1. Initial denaturation	98	30
2. Denaturation	98	10
3. Annealing	60 / 55 / 54	20
4. Extension	72	30 / 60 / 35
30x repeat of steps 2-4		
5. Final extension	72	300

D Results from inhibitor titration experiment

The inhibitor titration yielded the cell densities after 2 days of inhibition as shown in Table D.1. The colchicine-treated culture showed almost full growth at the addition of 25 mM, and almost completely inhibited at 50 mM. For further treatments a concentration of 40 mM colchicine was used. The oryzaline-treated culture had a partial inhibition of growth at 0.2 mM, and so this concentration was used in further experiments. The cytochalasin D-culture had partially inhibited growth both at 3 and 6 mM, so the 6 mM concentration was used for further experiments.

Table D.1: The cell density of the cultures at the beginning of the titration experiment and 2 days after addition of inhibitor. A control culture with no addition of inhibitor is given for comparison.

Colchicine						
Inhibitor concentration [mM]	Start	Control	25	50	100	200
Cell density [cells/µ]	506	3 721	3 600	597	409	409
Oryzaline						
Inhibitor concentration [mM]	Start	Control	0.1	0.2	0.4	0.8
Cell density [cells/µ]	506	3 721	3 632	1 842	232	248
Cytochalasin D						
Inhibitor concentration [mM]	Start	Control	1.5	3	6	12
Cell density [cells/µ]	506	3 721	3 654	1 849	1 842	569

E Results from project thesis

This master's thesis is a continuation of a project thesis from the fall of 2019 (Gresseth, 2019). The thesis produced mNeonGreen-Tp24711 transformants that were studied using a confocal microscope and a synchronisation experiment, such as was done in this thesis. The results and a short summary are given in the following section.

In Figure E.1 two transformant cells are imaged. The mNeonGreen fluorescence is visible in the valve and in the region of the girdle bands.

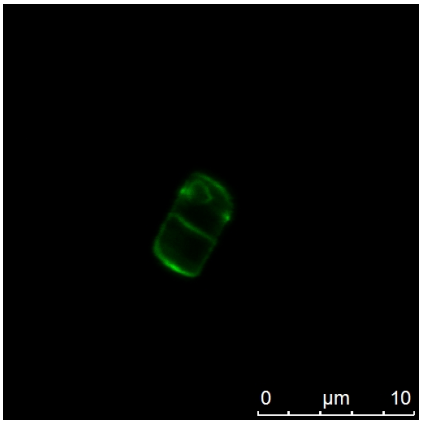

(a) 500-570 nm

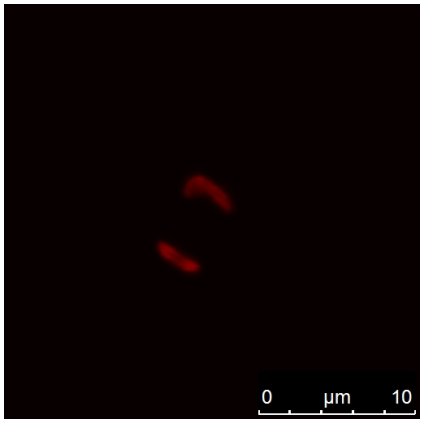

(b) >650 nm

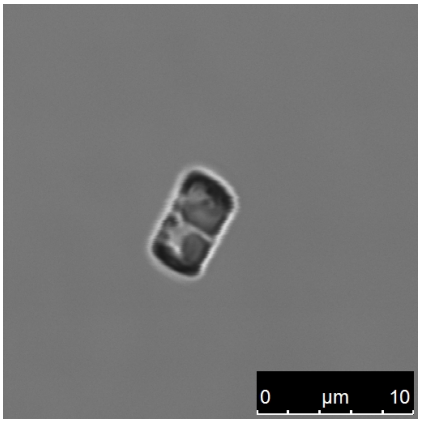

(c) Brightfield

Figure E.1: Confocal microscopy images of cells from a wild-type *T. pseudonana*. On the bottom right of each image is a scale bar to indicate the size of the cells. The fluorescence emitted from the cells emitted in the range of (a) mNeonGreen (500-570 nm) and (b) autofluorescence (>650 nm). (c) Brightfield imaging.

In Figure E.2 a single cell is shown. There is a clear region of mNeonGreen fluorescence in the girdle band region. Looking at Figure E.2b, the z-projection shows that the mNeonGreen fluorescence extends around the cingulum in a ring, which could be the equivalent of one girdle band.

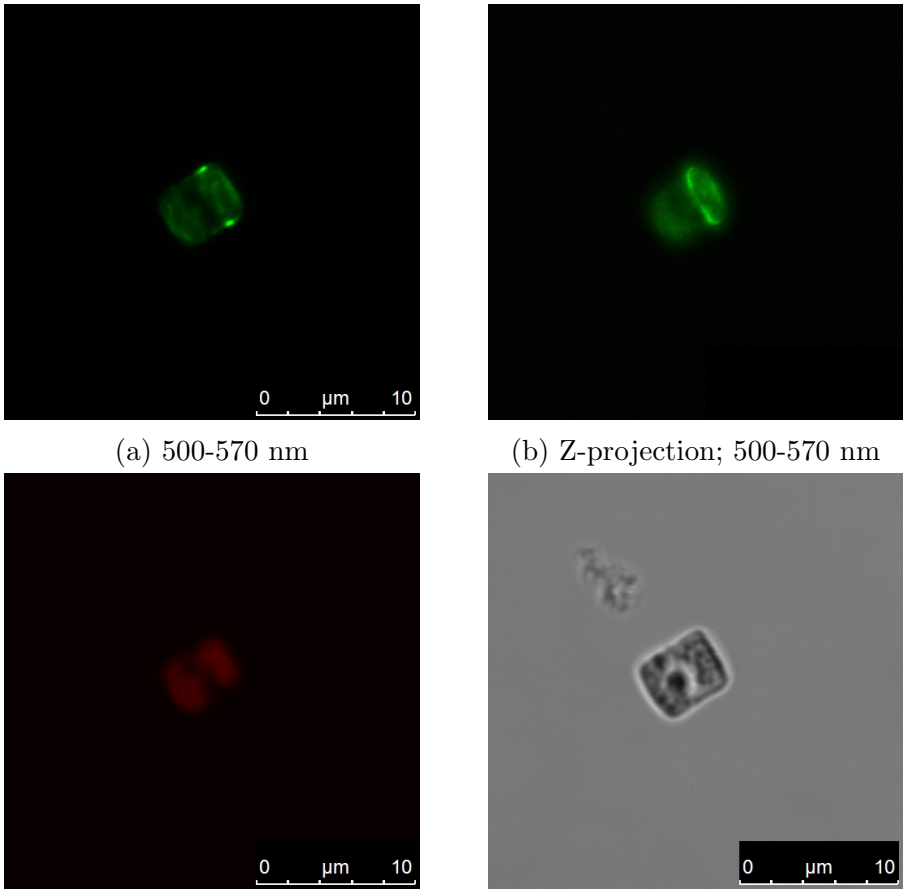

(a) 500-570 nm

(b) Z-projection; 500-570 nm

(c) >650 nm

(d) Brightfield

Figure E.2: Confocal microscopy images of cells from a wild-type *T. pseudonana*. On the bottom right of each image is a scale bar to indicate the size of the cells. The fluorescence emitted from the cells emitted in the range of (a) mNeonGreen and (b) autofluorescence. (c) Brightfield imaging.

The two figures show that mNeonGreen is expressed in the valve and the girdle bands, indicating a possible role for the Tp24711 protein in both valve and girdle band synthesis.

The data from the synchronisation experiment is given in Figure E.3 Datapoint 0h and 6h were discarded, because they did not add up with the rest of the curve. In the synchronisation experiment the cells were arrested

in the cell cycle check point G2 in stead of in G1 (Figure E.3a), which lead to cell divisions in the beginning of the experiment. The fluorescence for the transformants was highest in the beginning of the experiment, which was estimated to be the G2/M phase.

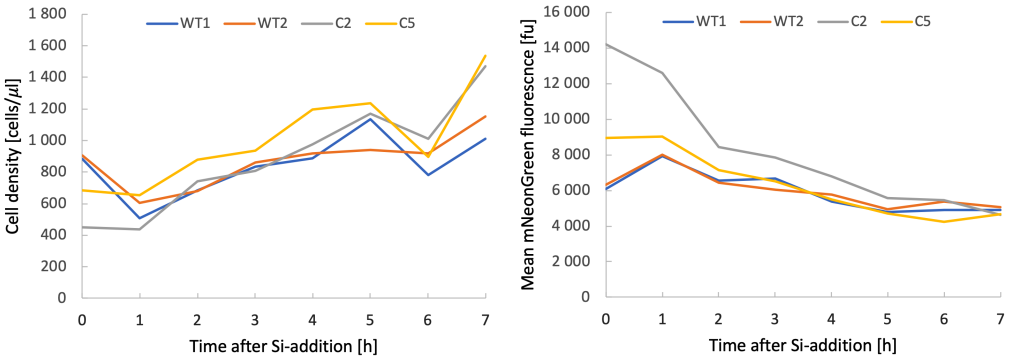

(a) Cell density

(b) Mean mNeonGreen fluorescence

Figure E.3: The (a) cell density and (b) mean mNeonGreen fluorescence in the cultures as a function of time after Si was added to the medium. WT1 and WT2 are two cultures of wild-type *T. pseudonana*, and C2 and C5 are Tp24711-mNeonGreen transformant clones 2 and 5, respectively.

NTNU

Norwegian University of
Science and Technology